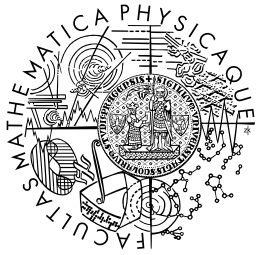

FACULTY
OF MATHEMATICS
AND PHYSICS
Charles University

BACHELOR THESIS

Jakub Dolejší

Dynamics of externally driven quantum systems

Institute of Particle and Nuclear Physics

Supervisor of the bachelor thesis:	prof. RNDr. Pavel Cejnar, Dr., DSc.
Study programme:	Physics
Study branch:	General Physics

Prague 2018

I declare that I carried out this bachelor thesis independently, and only with the cited sources, literature and other professional sources.

I understand that my work relates to the rights and obligations under the Act No. 121/2000 Sb., the Copyright Act, as amended, in particular the fact that the Charles University has the right to conclude a license agreement on the use of this work as a school work pursuant to Section 60 subsection 1 of the Copyright Act.

In Prague, May 17, 2018 Jakub Dolejší

I would like to express my gratitude to my supervisor prof. Pavel Cejnar for his guidance and constructive criticism.

I thank my family and friends for making my life joyful.

Title: Dynamics of externally driven quantum systems

Author: Jakub Dolejší

Institute: Institute of Particle and Nuclear Physics

Supervisor: prof. RNDr. Pavel Cejnar, Dr., DSc., Institute of Particle and Nuclear Physics

Abstract: We present the concept of an excited-state quantum phase transition and analyse its influence on the non-equilibrium dynamics after a quantum quench in the Lipkin model. We show that if the energy distribution of the initial state after the quench is centred at the critical energy, the survival probability of the initial state evolves in an anomalous way.

Keywords: Quantum phase transitions, Excited-state quantum phase transitions, Quantum quenches, Lipkin model

Název práce: Dynamika externě řízených kvantových systémů

Autor: Jakub Dolejší

Ústav: Ústav částicové a jaderné fyziky

Vedoucí bakalářské práce: prof. RNDr. Pavel Cejnar, Dr., DSc., Ústav částicové a jaderné fyziky

Abstrakt: Představujeme koncept kvantových fázových přechodů excitovaných stavů a zkoumáme jejich vliv na nerovnovážnou dynamiku po kvantovém kvenči v Lipkinově modelu. Ukazujeme, že pokud je po kvenči rozdělení energie původního stavu centrované na kritické energii, pak se pravděpodobnost přežití původního stavu vyvíjí anomálně.

Klíčová slova: Kvantové fázové přechody, Kvantové fázové přechody excitovaných stavů, Kvantové kvenče, Lipkinův model

Contents

Introduction

In most theories in physics, the equilibrium is the first aspect well-described, and for multiple reasons. Usually, quite a few properties can be deduced from knowing the system's equilibrium and a great deal of systems evolve in a fashion that tends towards the equilibrium. What happens frequently is that a system in a general initial state undergoes a quick transient phenomenon and then stabilizes in a (meta-)equilibrium which, in the long run, is the most significant state. A more pragmatic reason is that investigating only system equilibria is more simple than investigating the entire dynamics, and therefore the research begins there.

However, a negligibly fast decay into an equilibrium is by far not the only phenomenon to come by. In some cases, the exact course of a transition between states (or of any evolution in general) determines whether a new (distinct) effect will take place. It is also possible that a system will not even come close to any equilibrium. On that account, it is desirable to understand all dynamical properties of a theory and also their consequences.

In this thesis, we study dynamical properties of a quantum system out of equilibrium. In particular, we look into externally driven quantum systems. External driving means that the Hamiltonian of a system is set beforehand and is given as a definite function of time. Another method of probing the dynamics of a quantum system would be opening an initially closed system to interaction with the surrounding environment. In both cases, we begin with an eigenstate of the initial Hamiltonian and then change the Hamiltonian so that the state is out of equilibrium.

The dynamics strongly depends on the speed of the Hamiltonian change. To quantify the speed, assume that the Hamiltonian is a continuous function of a real control parameter λ which itself is a function of time. For an infinitely slow change of λ with time (i.e. $\frac{\mathrm{d}\lambda}{\mathrm{d}t} \ll 1$), which is called the adiabatic limit, the system will at all times stay in its instantaneous eigenstate. This effect is useful in adiabatic quantum computing. However, in reality, it is necessary that all processes last a finite amount of time.

We will focus on the opposite extreme which became known as a quantum quench. In this case the control parameter λ undergoes a sudden, diabatic change. After changing λ, the initial state will not be an eigenstate anymore and its evolution will be non-trivial. A possible way to describe the evolution is by observing the norm of the projection of the evolved state onto the initial one – the survival probability. Quantum quenches manifest several qualitatively distinct stages of time evolution of the survival probability.

Quantum quenches are often studied along with quantum phase transitions (QPTs) in order to distinguish between different phases by the quench dynamics. QPTs are critical phenomena in which a small change of the control parameter induces a macroscopic response of the system. Traditionally, a QPT refers to a critical phenomenon in the ground state. Excited-state quantum phase transitions (ESQPTs) represent a generalization of the concept to excited energy levels. The impact of an ESQPT on the system is rapidly weakened by a growth of the number of degrees of freedom f. Therefore, the ESQPT phenomenon requires

that a system exhibit collective behaviour – in which case f does not grow with the increase of the system size (the number of particles it consists of). Nevertheless, plenty of models incorporate it, e.g. the Lipkin-Meshkov-Glick model of a lattice of spins, the molecular vibron model which deals with vibrational modes of a molecule, the interacting boson model of a nucleus or the extended Dicke model used in quantum optics (see [1–3] and references therein). On the other hand, ground-state QPTs are quite common and are observed in plenty of interacting many-body systems, such as the Ising model or new alloys and materials [4].

We will conduct our investigations on the Lipkin model which was originally created as a toy model, but nowadays, it experiences a renewed attention of the scientific community. Rapid progress in quantum technologies enabled performing experiments on real-time quantum dynamics. These experiments are carried out by quantum simulators, which have been realized, for instance on ultra-cold atoms, trapped ions or superconducting qubits [5]. The Lipkin model is experimentally well-handled and can be finely tuned. It, therefore, provides a way to experimentally verify theoretical predictions.

1. Quantum phase transitions

1.1 Ground-state quantum phase transitions

Every physics problem depends on various parameters (e.g. external field intensity, internal interaction strength or surrounding material properties). Consider a Hamiltonian $\hat{H}$ with a real control parameter λ in the following form,

$$\hat{H}(\lambda) = \hat{H}_0 + \lambda \hat{V}\,, \tag{1.1}$$

where $\hat{H}_0$ represents a free Hamiltonian and $\hat{V}$ is an interaction Hamiltonian. Assume $\hat{H}$ has discrete energy spectrum. Furthermore, assume that $\left[\hat{H}_0, \hat{V}\right] \neq 0$, otherwise the eigenstates of $\hat{H}(\lambda)$ would not depend on λ and their respective energies would depend linearly on λ (i.e., there would not be any phase transition).

A *quantum phase transition* is defined as a non-analyticity in the energy of the ground state at a critical value λ_c of the control parameter (other than temperature). Strictly said, the singularity in an energy derivative occurs only in the limit of infinite system size (number of constituents). However, the system manifests definite signs of critical behaviour even for finite sizes.

Let us introduce the Ehrenfest classification of QPTs by types of the non-analyticity. In an *n-th order* QPT, the n-th derivative of the ground-state energy $\frac{\mathrm{d}^n}{\mathrm{d}\lambda^n} E_\lambda^{\mathrm{gs}}$ exhibits a jump discontinuity at λ_c and all its lower-order derivatives are continuous. In particular, a first-order QPT means that the ground-state energy is continuous but non-smooth at λ_c, which corresponds to a jump discontinuity in the first derivative. However, the Ehrenfest classification fails in many realistic cases in which the corresponding derivative does not exist at all.

An equivalent approach to QPTs is by the behaviour of observables as a function of λ. *Order parameter* O is such an observable by whose value it is possible to distinguish among different phases. It is customary to choose O so that it has zero value in one of the phases. A jump discontinuity (or non-existence) in the l-th derivative of E_λ^{gs} is equivalent to a jump discontinuity (or non-existence) in the $(l-1)$th derivative of the order parameter.

It is possible to introduce a more general classification of QPTs. The names of the classes are based on the behaviour of the order parameter. A *discontinuous* QPT is characterized by a discontinuity in O at λ_c and it corresponds to a first-order QPT. Whereas *continuous* QPTs are characterized by a continuous order parameter O with either a jump discontinuity or a non-existence in any of the higher derivatives. Thus, all QPTs of order higher than two are continuous.

1.2 Excited-state quantum phase transitions

An *excited-state quantum phase transition* represents a generalization of a QPT to higher energy levels. It refers to a non-analyticity in the energy spectrum of excited states. The characterisation of different phases delimited by an ESQPT is more difficult than in a ground-state QPT. It does not have to show up as a non-analyticity of single states. Instead, the expectation value of different observables as a smoothed function of energy show abrupt qualitative changes at the ESQPT

critical energy [3]. The most significant such quantity is the smoothed energy level density $\bar{\rho}$.

Both ground-state QPTs and ESQPTs have to do with the behaviour of the corresponding classical Hamiltonian. QPTs are the result of non-analyticities with respect to λ in the global minimum of the classical Hamiltonian, whereas ESQPTs relate to its stationary points at energies higher than its global minimum [2]. The critical borderline (*separatrix*) in $E \times \lambda$ plane which indicates the ESQPT often intersects the ground-state QPT [1, 3].

Article [2] shows that it is not possible to classify ESQPTs corresponding to degenerate stationary points. Whereas, ESQPTs corresponding to non-degenerate stationary points in the classical Hamiltonian (i.e., the Hessian matrix has a non-zero determinant) can be classified based on the number of system's degrees of freedom f and the rank r of the stationary point (the number of Hessian negative eigenvalues). The predicted behaviour of the smoothed energy density in vicinity of the critical energy E_c (which itself depends on λ) is

$$\frac{\partial^{f-1}\bar{\rho}}{\partial E^{f-1}} \propto \begin{cases} (-1)^{\frac{r+1}{2}} \log|E - E_\mathrm{c}| & \text{for } r \text{ odd}\,, \\ (-1)^{\frac{r}{2}} \quad \theta(E - E_\mathrm{c}) & \text{for } r \text{ even}\,, \end{cases} \tag{1.2}$$

where θ is the Heaviside step function. Therefore, an ESQPT manifests itself either as a logarithmic divergence or a jump discontinuity in the $(f-1)$th derivative of the smoothed energy level density. The effect of ESQPTs grows weaker as f increases (the singularity is shifted to higher derivatives). Thus, ESQPTs occur in infinite-size many-body systems with a finite number of degrees of freedom. This statement implies that the system must exhibit some kind of collective behaviour [1].

In the following, we will mostly deal with ESQPTs of type $(f, r) = (1, 1)$, i.e. a local maximum in a two-dimensional Hamiltonian ($\dim = 2f$) which manifests itself as divergence in the smoothed density of states. In a corresponding finite-size system, the ESQPT generates only a steeply higher density of states. However, the Hamiltonian eigenstates do not cross each other in spite of the high density. With increasing λ, they only get closer and then draw apart, once again. This phenomenon is called the *avoided crossing*. A derivation that the eigenstates undergo only avoided crossings can be seen in appendix A.

Classical correspondence

Assume a classical particle moving in a potential given by the classical Hamiltonian. If it has energy equal to that of a potential maximum, its velocity in the vicinity of the potential maximum is close to zero. This implies high probability of finding the particle in the vicinity of the potential maximum.

The quantum density of states at energy E is proportional to the period of a classical motion along a closed trajectory corresponding to energy E. The only possible trajectory for the critical energy is pathological and the particle reaches the potential maximum in infinite time. Therefore, the corresponding period is infinite and so is the density of states.

2. Quantum quench dynamics

2.1 Quantum quench

A quantum quench is a protocol in which the system is prepared in an eigenstate of the initial Hamiltonian $\hat{H}_\mathrm{i}$ and then the state is exposed to a sudden change of the Hamiltonian from $\hat{H}_\mathrm{i}$ to $\hat{H}_\mathrm{f}$. Say, this instantaneous change happens at time 0 and the state then evolves for a given period of time t in the final Hamiltonian $\hat{H}_\mathrm{f}$.

Assume a more general Hamiltonian in the form of (1.1) which satisfies, for two distinct values of the control parameter λ_i and λ_f, the following,

$$\hat{H}_\mathrm{i} = \hat{H}(\lambda_\mathrm{i})\,, \tag{2.1}$$

$$\hat{H}_\mathrm{f} = \hat{H}(\lambda_\mathrm{f})\,. \tag{2.2}$$

Let us denote $\left|\psi^{(k)}_{\mathrm{i,f}}\right\rangle$ the eigenstate of $\hat{H}_\mathrm{i,f}$ with the k-th energy $E^{(k)}_\mathrm{i,f}$. The initial state of the system is chosen so that

$$|\psi(0)\rangle = \left|\psi^{(k)}_\mathrm{i}\right\rangle\,. \tag{2.3}$$

Therefore, the resulting state after the evolution in $\hat{H}_\mathrm{f}$ is given by the Schödinger equation as

$$|\psi(t)\rangle = \hat{U}(t)\,|\psi(0)\rangle = \mathrm{e}^{-i\hat{H}_\mathrm{f}t}\,|\psi(0)\rangle\,, \tag{2.4}$$

where we assumed $\hbar = 1$.

2.2 Survival probability

Survival probability $P(t)$ (also called the *Loschmidt echo*) is the probability that $|\psi(t)\rangle$ will be identified as $|\psi(0)\rangle$,

$$P(t) = \left|\,\langle\psi(0)|\psi(t)\rangle\,\right|^2 = \left|\left\langle\psi(0)\middle|\mathrm{e}^{-i\hat{H}_\mathrm{f}t}\middle|\psi(0)\right\rangle\right|^2\,. \tag{2.5}$$

The corresponding probability amplitude is called the *Loschmidt amplitude*,

$$\mathcal{G}(t) = \left\langle\psi(0)\middle|\mathrm{e}^{-i\hat{H}_\mathrm{f}t}\middle|\psi(0)\right\rangle\,. \tag{2.6}$$

Fidelity $f(t)$ is the probability amplitude that the quenched and evolved state $|\psi(t)\rangle$ will be identified as state $|\psi_\mathrm{i}(t)\rangle$ obtained by evolving the same initial state for the same amount of time t but in the initial Hamiltonian $\hat{H}_\mathrm{i}$,

$$\mathcal{F}(t) = \langle\psi_\mathrm{i}(t)|\psi(t)\rangle = \left\langle\psi(0)\middle|\mathrm{e}^{+i\hat{H}_\mathrm{i}t}\mathrm{e}^{-i\hat{H}_\mathrm{f}t}\middle|\psi(0)\right\rangle\,. \tag{2.7}$$

Thanks to (2.3), fidelity relates to the previous two quantities in the following manner,

$$\mathcal{F}(t) = \mathrm{e}^{+iE^{(k)}_\mathrm{i}t}\left\langle\psi(0)\middle|\mathrm{e}^{-i\hat{H}_\mathrm{f}t}\middle|\psi(0)\right\rangle = \mathrm{e}^{+iE^{(k)}_\mathrm{i}t}\mathcal{G}(t)\,, \tag{2.8}$$

$$|\mathcal{F}(t)|^2 = |\mathcal{G}(t)|^2 = P(t)\,. \tag{2.9}$$

2.3 Strength function

Let us define coefficients s_k as the projections of the initial state onto the eigenbasis of the final Hamiltonian,

$$|\psi(0)\rangle = \sum_k \left\langle \psi_{\mathrm{f}}^{(k)} \middle| \psi(0) \right\rangle \left| \psi_{\mathrm{f}}^{(k)} \right\rangle \equiv \sum_k s_k \left| \psi_{\mathrm{f}}^{(k)} \right\rangle , \tag{2.10}$$

where k iterates through the total number d of system eigenstates (the system dimension). The final state $|\psi(t)\rangle$ can then be expressed as

$$|\psi(t)\rangle = \mathrm{e}^{-i\hat{H}_{\mathrm{f}}t} \sum_k s_k \left| \psi_{\mathrm{f}}^{(k)} \right\rangle = \sum_k s_k \mathrm{e}^{-iE_{\mathrm{f}}^{(k)}t} \left| \psi_{\mathrm{f}}^{(k)} \right\rangle . \tag{2.11}$$

It is also possible to define *strength function* $S(E)$ as the energy distribution of the initial state among $\hat{H}_{\mathrm{f}}$ eigenstates,

$$S(E) = \sum_k |s_k|^2 \, \delta\left(E - E_{\mathrm{f}}^{(k)}\right) . \tag{2.12}$$

Since the strength function represents an energy distribution, it is possible to compute the mean energy and its variance for the initial state in the final Hamiltonian,

$$\langle E_{\mathrm{f}} \rangle_{\mathrm{i}} = \int S(E) E \, \mathrm{d}E = \sum_k |s_k|^2 \, E_{\mathrm{f}}^{(k)} , \tag{2.13}$$

$$\left\langle\left\langle E_{\mathrm{f}}^2 \right\rangle\right\rangle_{\mathrm{i}} = \int S(E) \left(E - \langle E_{\mathrm{f}} \rangle_{\mathrm{i}}\right)^2 \mathrm{d}E = \sum_k |s_k|^2 \left(E_{\mathrm{f}}^{(k)} - \langle E_{\mathrm{f}} \rangle_{\mathrm{i}}\right)^2 . \tag{2.14}$$

We can write the survival probability in terms of the strength function as

$$P(t) = \left| \langle \psi(0) | \psi(t) \rangle \right|^2 = \left| \sum_k |s_k|^2 \mathrm{e}^{-iE_{\mathrm{f}}^{(k)}t} \right|^2 = \left| \int S(E) \mathrm{e}^{-iEt} \, \mathrm{d}E \right|^2 . \tag{2.15}$$

Thus, all the information contained in the survival probability as a function of time is equivalently concealed in the strength function $S(E)$ and one can reconstruct $P(t)$ from knowing $S(E)$.

By computing the absolute value in the expression after the second equality sign in (2.15),

$$P(t) = \sum_k |s_k|^4 + 2 \sum_k \sum_{k'<k} |s_k|^2 |s_{k'}|^2 \cos\left(\left(E_{\mathrm{f}}^{(k)} - E_{\mathrm{f}}^{(k')}\right) t\right) , \tag{2.16}$$

it is easy to see, that on large time scales, the survival probability will oscillate around a non-zero value $\mathcal{N}^{-1} \equiv \sum_k |s_k|^4$. The quantity $\mathcal{N}$ is called the *participation ratio* and it quantifies the level of delocalization of state $|\psi(0)\rangle$ in $\hat{H}_{\mathrm{f}}$ eigenstates [6, 7],

$$\mathcal{N} = \frac{1}{\sum_k |s_k|^4} . \tag{2.17}$$

Its minimum value 1 corresponds to the case that $|\psi(0)\rangle$ is one of the basis states. The maximum value, which is equal to the system dimension d, corresponds to a state evenly distributed among $\hat{H}_{\mathrm{f}}$ basis states. In the latter case $|s_k|^2 = \frac{1}{d}$.

2.4 Designing quench protocols

Knowing the mean energy of the initial state $\left|\psi_{\mathrm{i}}^{(k)}\right\rangle$ in the final Hamiltonian $\hat{H}_{\mathrm{f}}$ would enable us to design specific quench protocols that probe any spectrum area chosen beforehand. Computing the λ-derivative of the eigenenergy $E_{\lambda}^{(k)}$ of a general Hamiltonian (1.1) will ultimately allow us to do so.

Eigenenergy $E_{\lambda}^{(k)}$ can be expressed as

$$E_{\lambda}^{(k)} = \left\langle \psi_{\lambda}^{(k)} \middle| \hat{H}(\lambda) \middle| \psi_{\lambda}^{(k)} \right\rangle . \tag{2.18}$$

After differentiating equation (2.18) with respect to λ, we obtain

$$\begin{aligned}
\frac{\mathrm{d}E_{\lambda}^{(k)}}{\mathrm{d}\lambda} &= \left\langle \frac{\mathrm{d}}{\mathrm{d}\lambda}\psi_{\lambda}^{(k)} \middle| \hat{H}(\lambda) \middle| \psi_{\lambda}^{(k)} \right\rangle + \left\langle \psi_{\lambda}^{(k)} \middle| \hat{H}(\lambda) \middle| \frac{\mathrm{d}}{\mathrm{d}\lambda}\psi_{\lambda}^{(k)} \right\rangle + \left\langle \psi_{\lambda}^{(k)} \middle| \frac{\mathrm{d}\hat{H}}{\mathrm{d}\lambda} \middle| \psi_{\lambda}^{(k)} \right\rangle = \\
&= E^{(k)}(\lambda) \left[\left\langle \frac{\mathrm{d}}{\mathrm{d}\lambda}\psi_{\lambda}^{(k)} \middle| \psi_{\lambda}^{(k)} \right\rangle + \left\langle \psi_{\lambda}^{(k)} \middle| \frac{\mathrm{d}}{\mathrm{d}\lambda}\psi_{\lambda}^{(k)} \right\rangle \right] + \left\langle \psi_{\lambda}^{(k)} \middle| \hat{V} \middle| \psi_{\lambda}^{(k)} \right\rangle = \\
&= E^{(k)}(\lambda) \frac{\mathrm{d}}{\mathrm{d}\lambda} \underbrace{\left\langle \psi_{\lambda}^{(k)} \middle| \psi_{\lambda}^{(k)} \right\rangle}_{1} + \left\langle \psi_{\lambda}^{(k)} \middle| \hat{V} \middle| \psi_{\lambda}^{(k)} \right\rangle = \\
&= \left\langle \psi_{\lambda}^{(k)} \middle| \hat{V} \middle| \psi_{\lambda}^{(k)} \right\rangle ,
\end{aligned} \tag{2.19}$$

which is called the Hellmann-Feynman formula.

Now, with the use of (2.18) and (2.19), we can write the mean energy of the initial state in the final Hamiltonian,

$$\langle E_{\mathrm{f}} \rangle_{\mathrm{i}} = \left\langle \psi_{\mathrm{i}}^{(k)} \middle| \hat{H}_{\mathrm{f}} \middle| \psi_{\mathrm{i}}^{(k)} \right\rangle = \left\langle \psi_{\mathrm{i}}^{(k)} \middle| \hat{H}_{\mathrm{i}} + \Delta\lambda \hat{V} \middle| \psi_{\mathrm{i}}^{(k)} \right\rangle = E_{\mathrm{i}}^{(k)} + \left. \frac{\mathrm{d}E_{\lambda}^{(k)}}{\mathrm{d}\lambda} \right|_{\lambda_{\mathrm{i}}} \Delta\lambda , \tag{2.20}$$

where $\Delta\lambda = \lambda_{\mathrm{f}} - \lambda_{\mathrm{i}}$. Thus, quenching can be interpreted as moving along a tangent between points λ_{i} and λ_{f} in the graph of energy levels as a function of control parameter λ.

Let us examine the energy variance of the resulting state,

$$\begin{aligned}
\left\langle\left\langle E_{\mathrm{f}}^2 \right\rangle\right\rangle_{\mathrm{i}} &= \left\langle \psi_{\mathrm{i}}^{(k)} \middle| \hat{H}_{\mathrm{f}}^2 \middle| \psi_{\mathrm{i}}^{(k)} \right\rangle - \left\langle \psi_{\mathrm{i}}^{(k)} \middle| \hat{H}_{\mathrm{f}} \middle| \psi_{\mathrm{i}}^{(k)} \right\rangle^2 = \\
&= \left\langle \psi_{\mathrm{i}}^{(k)} \middle| \left(E_{\mathrm{i}}^{(k)} + \Delta\lambda \hat{V} \right)^2 \middle| \psi_{\mathrm{i}}^{(k)} \right\rangle - \left(E_{\mathrm{i}}^{(k)} + \Delta\lambda \left\langle \psi_{\mathrm{i}}^{(k)} \middle| \hat{V} \middle| \psi_{\mathrm{i}}^{(k)} \right\rangle \right)^2 = \\
&= \Delta\lambda^2 \left\langle\left\langle \hat{V}^2 \right\rangle\right\rangle_{\mathrm{i}} ,
\end{aligned} \tag{2.21}$$

where we used $\hat{H}_{\mathrm{f}} = \hat{H}_{\mathrm{i}} + \Delta\lambda\hat{V}$ together with $\hat{H}_{\mathrm{i}} \left|\psi_{\mathrm{i}}^{(k)}\right\rangle = E_{\mathrm{i}}^{(k)} \left|\psi_{\mathrm{i}}^{(k)}\right\rangle$.

Equation (2.20) truly enables us to construct any desired quench protocol. We are particularly interested in quenching between distinct quantum phases. On the other hand, we cannot quench over too large $\Delta\lambda$ because the energy variance of the final state is proportional to $\Delta\lambda^2$ and we could get a state extended over a too large energy interval (in the worst scenario over multiple quantum phases).

2.5 Regimes of quench dynamics

The evolution of the survival probability can be divided into different regimes on different time scales [6]. At first, the dynamics is determined solely by the energy distribution variance. Later, with proceeding time, the evolution of the system is given by more and more subtle details of the strength function (such as its outline or discrete structure).

Let us estimate the time scale when the system starts to behave according to the discrete structure of the energy distribution (*the Heisenberg time*). To this purpose, we exploit the time-energy uncertainty principle (remember that we have $\hbar = 1$),

$$t_{\mathrm{H}} = \frac{2\pi}{\langle \Delta E_{\mathrm{f}} \rangle_{\mathrm{i}}}\,, \tag{2.22}$$

where $\langle \Delta E_{\mathrm{f}} \rangle_{\mathrm{i}}$ is the average energy level spacing of the initial state in the final Hamiltonian. There are multiple ways to determine the reasonable value of $\langle \Delta E_{\mathrm{f}} \rangle_{\mathrm{i}}$. We will stick with [6], where the difference of neighbouring energy levels is weighted by the sum of their respective eigenstates participation in the initial state,

$$\langle \Delta E_{\mathrm{f}} \rangle_{\mathrm{i}} = A \sum_k \left(|s_{k+1}|^2 + |s_k|^2 \right) \left(E_{\mathrm{f}}^{(k+1)} - E_{\mathrm{f}}^{(k)} \right)\,, \tag{2.23}$$

where the sum goes over all $d-1$ neighbouring eigenenergy differences. The normalizing factor A ensures that the sum of the weight coefficients is equal to one,

$$A = \frac{1}{\sum_k \left(|s_{k+1}|^2 + |s_k|^2 \right)} = \frac{1}{2 - |s_1|^2 - |s_d|^2}\,. \tag{2.24}$$

The evolution starts with the ultra-short regime, in which the survival probability is given as the second order Taylor series for (2.5),

$$P(t) \approx 1 - \left(\frac{t}{t_{\mathrm{s}}} \right)^2\,, \tag{2.25}$$

where $t_{\mathrm{s}} \equiv 1/\sqrt{\langle\langle E_{\mathrm{f}}^2 \rangle\rangle_{\mathrm{i}}}$. The expansion is valid for $t \ll t_{\mathrm{s}}$. In this regime, the decay is determined solely by the energy distribution variance.

In short- and medium-time regime from $t \sim t_{\mathrm{s}}$ up to $t \ll t_{\mathrm{H}}$, the system evolution is given by the energy distribution outline. The initial decay is predicted to be exponential, Gaussian or sub-Gaussian. Thus, comparing the real Loschmidt echo with the approximating Gaussian,

$$P(t) \approx \exp\left(- \left(\frac{t}{t_{\mathrm{s}}} \right)^2 \right), \tag{2.26}$$

provides some insight into the decay speed. Then, power-law modulated oscillations may occur.

Long-time regime around $t \sim t_{\mathrm{H}}$ is given by the discrete structure of energy eigenstates. Power-law modulated oscillations may occur in this phase, too. A long-lasting decrease in the survival probability (below the infinite time average) may follow.

In the ultra-long-time regime, $t \gg t_{\mathrm{H}}$, the survival probability fluctuates around the mean value $\overline{P(t)} = \mathcal{N}^{-1}$ as given by (2.16). Irrespective of the usually low average $\overline{P(t)}$, sharp peaks of the near initial-state recovery arise in this phase.

3. Lipkin model

Simple Hamiltonians are used to manipulate with quantum systems (for example, in quantum computing) and it is, therefore, crucial that we know exactly what can happen under the action of such Hamiltonians. Some of these Hamiltonians exhibit critical behaviour like QPTs and possibly ESQPTs.

The Lipkin-Meshkov-Glick model (or the Lipkin model for short) [8], was created as a simple toy model of an atomic nucleus. A toy model means that it is used rather for exploring (quantum) phenomena than for describing reality with it. On the other hand, thanks to its simplicity, it can describe certain aspects of various complex models. The Lipkin model can be formulated by means of N interacting entities which can exist in one out of two possible states, e.g. spin-$\frac{1}{2}$ particles, fermions on two (N-fold degenerated) energy levels, two-level atoms, bosons of two different types. The Lipkin model also has a coordinate-momentum formulation (motion of a particle in a potential well).

3.1 Spin formulation

In the spin formulation we have a lattice of N interacting spins of size $\frac{1}{2}$. In the Lipkin model, the range of the spin interaction is infinite – which makes it an infinite-range limit of the Ising model [3].

We assign to the n-th spin a two dimensional Hilbert space $\mathcal{H}^{(n)}$ and a spin-$\frac{1}{2}$ operator (represented by Pauli matrices) $\hat{\boldsymbol{S}}^{(n)} = \frac{1}{2}\left(\hat{\sigma}_1^{(n)}, \hat{\sigma}_2^{(n)}, \hat{\sigma}_3^{(n)}\right)$ acting on it. Let us define the total spin operator

$$\hat{\boldsymbol{J}} = \sum_{n=1}^{N} \hat{\boldsymbol{S}}^{(n)} \tag{3.1}$$

acting on the whole spin lattice represented by $\mathcal{H} = \bigotimes_{n=1}^{N} \mathcal{H}^{(n)}$.

The potential energy of a spin $\hat{\boldsymbol{S}}^{(n)}$ in a magnetic field $\boldsymbol{B}$ is given as $\hat{V}_0^{(n)} = -g\mu\boldsymbol{B} \cdot \hat{\boldsymbol{S}}^{(n)}$, where g is the gyromagnetic ratio and μ is the Bohr magneton or nuclear magneton (whichever corresponds to the nature of the spins). The potential energy of the spin lattice $\hat{V}_0$ can be expressed by means of the collective spin $\hat{\boldsymbol{J}}$ for a homogeneous $\boldsymbol{B}$ as follows

$$\hat{V}_0 = \sum_{n=1}^{N} \hat{V}_0^{(n)} = -g\mu\boldsymbol{B} \cdot \left(\sum_{n=1}^{N} \hat{\boldsymbol{S}}^{(n)}\right) = -g\mu\boldsymbol{B} \cdot \hat{\boldsymbol{J}}\,. \tag{3.2}$$

For simplicity, we will consider only $\hat{V}_0 = \hat{J}_3$. That is, we will consider a special case of the magnetic field in the direction z and such strength that $g\mu B = -1$.

The energy of two interacting spins is proportional to $\hat{\boldsymbol{S}}^{(n)} \cdot \hat{\boldsymbol{S}}^{(m)}$. Since the interaction in the Lipkin model is infinite-range and we assume that each pair of spins interact with equal strength, the overall interaction energy can be written as

$$\hat{V}' \propto \sum_{m=1}^{N} \sum_{n=1}^{N} \hat{\boldsymbol{S}}^{(m)} \cdot \hat{\boldsymbol{S}}^{(n)} = \hat{\boldsymbol{J}}^2 \equiv \hat{J}^2\,. \tag{3.3}$$

Because $\bigotimes_{n=1}^{N} \left|s^{(n)}, m^{(n)}\right\rangle \equiv \bigotimes_{n=1}^{N} \left|\frac{1}{2}, m^{(n)}\right\rangle$ forms a basis of $\mathcal{H}$, the diagonal terms in (3.3) introduce only an additive constant which shifts the eigenenergies but which does not have an impact on the system dynamics,

$$\begin{aligned}\sum_{n=1}^{N} \hat{\boldsymbol{S}}^{(n)} \cdot \hat{\boldsymbol{S}}^{(n)} = \sum_{n=1}^{N} \left(\hat{S}^{(n)}\right)^2 = \sum_{n=1}^{N} s^{(n)} \left(s^{(n)}+1\right) \hat{\mathbb{I}} = \\ = \sum_{n=1}^{N} \frac{1}{2}\left(\frac{1}{2}+1\right) \hat{\mathbb{I}} = \frac{3}{4} N \hat{\mathbb{I}}\,,\end{aligned} \tag{3.4}$$

where $\hat{\mathbb{I}}$ is the identity operator.

Once again, we will consider only the first component $\hat{J}_1^2$ for the sake of simplicity. This invalidates the reasoning in (3.4) for a general spin size but $\frac{1}{2}$. The correct argument in this case is that the square of any Pauli matrix is equal to the identity and it follows that

$$\sum_{n=1}^{N} \hat{S}_1^{(n)} \hat{S}_1^{(n)} = \frac{1}{4} \sum_{n=1}^{N} \left(\hat{\sigma}_1^{(n)}\right)^2 = \frac{1}{4} N \hat{\mathbb{I}}\,. \tag{3.5}$$

The Lipkin model, in general, covers a class of Hamiltonians that can be expressed in terms of linear and quadratic terms of a quasispin operator components $\hat{J}_i$. Such Hamiltonians conserve $\hat{J}^2$ eigenvalue j because $\left[\hat{J}^2, \hat{J}_i\right] = 0$. We will consider one of the most common Lipkin Hamiltonians

$$\hat{H} = \hat{J}_3 + \lambda \left(-\frac{1}{2j} \hat{J}_1^2\right)\,, \tag{3.6}$$

which is in the form of (1.1). Control parameter λ represents the spin-spin interaction strength. We will refer to Hamiltonian (3.6) as the Lipkin Hamiltonian. From now on, let us consider only positive values of control parameter λ.

Describing the spin lattice by a collective spin, the original Hilbert space $\mathcal{H}$ of dimension 2^N falls apart into a direct sum of spin subspaces $\mathcal{H}_j$ with dimensions $2j+1$ for j between $j_{\min}$ and $j_{\max} = \frac{N}{2}$, where $j_{\min} = 0$ for N even or $j_{\min} = \frac{1}{2}$ for N odd. Because $\sum_{j_{\min}}^{j_{\max}} 2j+1 = \mathcal{O}(N^2)$ which is much less than 2^N, for large N, the subspaces $\mathcal{H}_j$ have to occur with a high multiplicity α_j in the whole Hilbert space $\mathcal{H}$ so that the equality of dimensions could be satisfied.

The subspace with the highest j (equal to $\frac{N}{2}$) contains the state in which all spins are directed up, and therefore it is unique ($\alpha_{N/2} = 1$). All lower Hilbert spaces $\mathcal{H}_j$ occur with a multiplicity given by the number of ways the constituent spins can be arranged so that the total spin of the lattice is j, minus the contribution from higher-j subspaces [3]. Mathematically speaking, $\mathcal{H} = \bigoplus_{j=j_{\min}}^{N/2} \bigoplus_{i=1}^{\alpha_j} \mathcal{H}_j^{(i)}$. Subspaces $\mathcal{H}_j^{(i)}$ with distinct index i differ in the exchange symmetry of the individual spins.

Each $\mathcal{H}_j = \bigoplus_{i=1}^{\alpha_j} \mathcal{H}_j^{(i)}$ is invariant under any Lipkin Hamiltonian for it conserves j. Consequently, we can restrict ourselves on any of the subspaces $\mathcal{H}_j$. It is customary to choose the highest-j subspace $\mathcal{H}_{N/2}$ of dimension $N+1$. After the restriction on any $\mathcal{H}_j$ the Hamiltonian represents a system with only one degree of freedom – the $\hat{J}_3$ eigenvalue.

The highest-j state $\left|\frac{N}{2}, \frac{N}{2}\right\rangle$ of the subspace $\mathcal{H}_{N/2}$ is totally symmetric with respect to the exchange of the constituent spins. The rest of the states from

$\mathcal{H}_{N/2}$ can be obtained by applying the lowering operator $\hat{J}_-$ on $\left|\frac{N}{2}, \frac{N}{2}\right\rangle$,

$$\hat{J}_- = \hat{J}_1 - i\hat{J}_2 \,. \tag{3.7}$$

Thanks to (3.1), it is possible to express the collective lowering operator in terms of lowering operators $\hat{S}_-^{(n)} = \hat{S}_1^{(n)} - i\hat{S}_2^{(n)}$ acting on the individual spins,

$$\hat{J}_- = \sum_{n=1}^{N} \hat{S}_-^{(n)} \,. \tag{3.8}$$

Now, we see that $\hat{J}_-$ acts on all spins in the same fashion. Thus, the whole subspace $\mathcal{H}_{N/2}$ is totally symmetric under the exchange of individual spins and all spins behave in the same way, or equivalently they exhibit collective behaviour.

3.2 Coordinate-momentum formulation

An arbitrary Lipkin Hamiltonian restricted on $\mathcal{H}_j$ can be cast from the spin formulation to the coordinate-momentum formulation by a transformation of operators as described in [9]. The transformation consists of two steps, first from spin ladder operators (which shift $\hat{J}_3$ eigenvalue by ± 1 or 0)

$$\hat{J}_\pm = \hat{J}_1 \pm i\hat{J}_2 \,, \tag{3.9}$$

$$\hat{J}_0 = \hat{J}_3 \tag{3.10}$$

to boson creation and annihilation operators $\hat{b}^\dagger$, $\hat{b}$ and then to harmonic oscillator creation and annihilation operators $\hat{x} \pm i\hat{p}$ (with a prefactor setting the properties of the particular oscillator). The particular formulae are

$$\left(\hat{J}_-, \hat{J}_0, \hat{J}_+\right) \mapsto \left(\sqrt{2j - \hat{b}^\dagger\hat{b}}\;\hat{b},\; \hat{b}^\dagger\hat{b} - j,\; \hat{b}^\dagger\sqrt{2j - \hat{b}^\dagger\hat{b}}\right) , \tag{3.11}$$

$$\left(\hat{b}^\dagger, \hat{b}\right) \mapsto \sqrt{j}\,(\hat{x} - i\hat{p}, \hat{x} + i\hat{p}) \,. \tag{3.12}$$

Transformation (3.11) is chosen so that the commutation relation of boson operators $\left[\hat{b}, \hat{b}^\dagger\right] = 1$ is satisfied. The commutation relation of coordinate and momentum, as given by transformation (3.12), is

$$[\hat{x}, \hat{p}] = \frac{i}{2j} \,. \tag{3.13}$$

3.3 Classical limit

Quantum behaviour is encoded in non-zero commutators. The classical limit, which is usually obtained by taking $\hbar \to 0$, can be also acquired by setting all conceivable commutators to zero. For the commutator given by (3.13), it is possible to do so in the limit of infinite system size $N \to \infty$ (and equivalently $j \to \infty$).

The classical analogy of Hamiltonian (3.6) is obtained by casting it from the spin representation to the coordinate-momentum representation and taking the limit of infinite system size $N \to \infty$. This way, we obtain

$$\frac{H}{j} = \underbrace{-1 + (1-\lambda)x^2 + \frac{\lambda}{2}x^4}_{\frac{V(x)}{j}} + \underbrace{p^2\left(1 + \frac{\lambda}{2}x^2\right)}_{\frac{T(x,p)}{j}} . \tag{3.14}$$

Therefore, a classical analogy of the Lipkin model of a spin lattice in a magnetic field is the motion of a particle in a potential well of the form $V(x)$ as given by (3.14).

For general λ, the kinetic term T depends on the position. It can be interpreted as a position-dependent effective mass (at $x = 0$ equal to the real mass). Nevertheless, it is possible to get insight into the system dynamics by analysing the shape of the potential term $V(x)$. It represents a potential well which turns into a double well system at $\lambda > \lambda_c \equiv 1$. The potential for critical $\lambda = \lambda_c$ is a quartic oscillator, in contrast with the sub-critical $\lambda < \lambda_c$ which in the neighbourhood of $x = 0$ represents a harmonic oscillator. The Hamiltonian for $\lambda = 0$ is exactly that of a harmonic oscillator on the whole x-domain. The dependency of the potential on λ is shown in fig. 3.1.

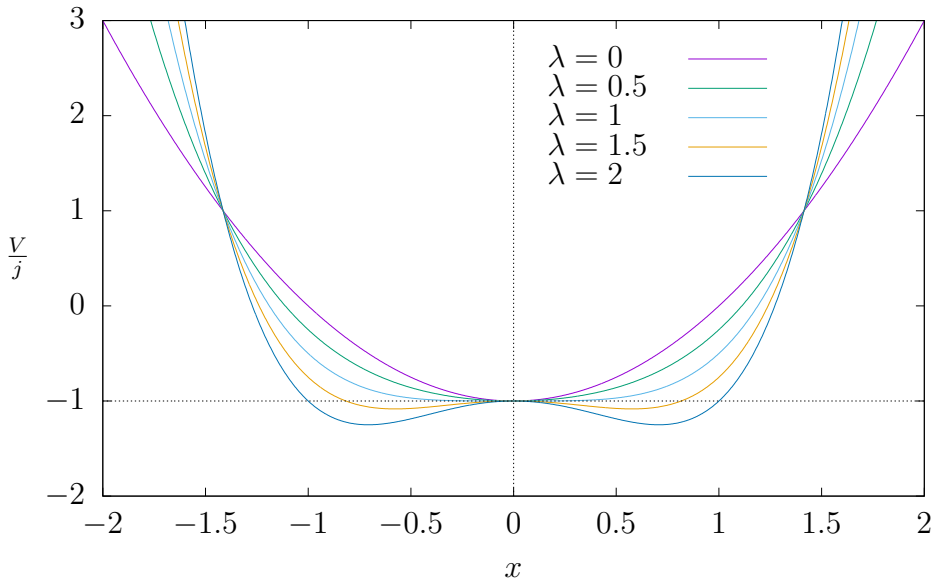

Figure 3.1: Classical potential corresponding to the Lipkin Hamiltonian

3.4 Quantum phase transition

Let us examine the Lipkin model Hamiltonian (3.6) for QPTs. First, we need to find the classical ground state, given as the global minimum of the function

$H(x,p)$. The conditions for stationary points of $H(x,p)$ are

$$0 = \frac{1}{j}\frac{\partial H}{\partial p} = 2p\left(1+\frac{\lambda}{2}x^2\right), \tag{3.15}$$

$$0 = \frac{1}{j}\frac{\partial H}{\partial x} = 2x(1-\lambda) + 2\lambda x^3 + p^2\lambda x\,. \tag{3.16}$$

By solving the set of these two equations we get two different types of solutions,

$$(x_1,p_1) = (0,0)\,, \tag{3.17}$$

$$(x_2,p_2) = \left(\pm\sqrt{\frac{\lambda-1}{\lambda}},0\right). \tag{3.18}$$

Both these solutions are in accord with the classical Hamiltonian equations of motion because

$$\dot{x}_{1,2} = \frac{\partial H}{\partial p}(x_{1,2}) = 0\,, \tag{3.19}$$

$$\dot{p}_{1,2} = -\frac{\partial H}{\partial x}(x_{1,2}) = 0\,, \tag{3.20}$$

and therefore a particle in any stationary point of the classical Hamiltonian is in rest and is not subject to any force. All in all, the particle can keep still in all the computed stationary points. On the other hand, the second solution (x_2,p_2) exists only for $\lambda > 1 \equiv \lambda_{\mathrm{c}}$.

To determine the overall ground state, we need to find the energies of the stationary points.

$$E_1 = H(x_1,0) = -j\,, \tag{3.21}$$

$$E_2 = H(x_2,0) = -j\left(1+\frac{(\lambda-1)^2}{2\lambda}\right). \tag{3.22}$$

Obviously, energy E_2 is smaller than E_1. However, both states exist at the same time only for $\lambda \geq \lambda_{\mathrm{c}}$. Hence the system ground state is given as

$$\frac{E^{\mathrm{gs}}(\lambda)}{j} = \begin{cases} -1 & \lambda \leq \lambda_{\mathrm{c}}\,, \\ -1-\frac{(\lambda-1)^2}{2\lambda} & \lambda \geq \lambda_{\mathrm{c}}\,. \end{cases} \tag{3.23}$$

Energy of the ground state given by formula (3.23) exhibits a jump discontinuity in the second derivative at $\lambda_{\mathrm{c}} = 1$. The energy itself and its first derivative are continuous thanks to the term $(\lambda-1)^2$. Therefore the QPT is of the second-order according to the Ehrenfest classification. We will come back to the derivatives of E^{gs} in table 3.1.

As proposed in [9], it is possible to choose the ground state spin inversion parameter (which represents the number of spin-up states) to be the order parameter,

$$\left\langle \hat{I} \right\rangle^{\mathrm{gs}} \equiv \langle \psi^{\mathrm{gs}} | \hat{J}_3 + j | \psi^{\mathrm{gs}} \rangle = j \left\langle \hat{x}^2 + \hat{p}^2 \right\rangle^{\mathrm{gs}}. \tag{3.24}$$

For $\lambda \leq \lambda_{\mathrm{c}}$, a particle in the ground state stays with zero momentum $p_1 = 0$ at $x_1 = 0$, which gives $\left\langle \hat{I} \right\rangle^{\mathrm{gs}} = 0$, zero number of spin-up states. That is, all spins are directed down and $\left\langle \hat{J}_3 \right\rangle^{\mathrm{gs}} = -\frac{N}{2} = -j$.

For $\lambda > \lambda_c$, the particle is in a superposition of keeping still in the left well and keeping still in the right well. Since the potential is symmetric, both minima are populated equally. Their distance from the origin of coordinates is $x_2 = \pm\sqrt{1-\frac{1}{\lambda}}$. Thus, the spin inversion parameter above the critical value λ_c reads as $\left\langle \hat{I} \right\rangle^{gs} = jx_2^2 = j\left(1-\frac{1}{\lambda}\right)$. Now, the constituent spins have a non-zero fraction in the up-direction.

The ground state spin inversion grows with increasing λ. The maximum value of $\left\langle \hat{I} \right\rangle^{gs}$ corresponds to $\lambda \to \infty$ and is equal to j. In that case, it is possible to write $\left\langle \hat{J}_3 \right\rangle^{gs} = \left\langle \hat{I} \right\rangle^{gs} - j = 0$, and so, the spins don't have any preferred direction in the z component in the limit of infinite spin interaction strength (since λ in Hamiltonian (1.1) represents the spin interaction strength). This phenomenon is expected because the effect of magnetic field becomes negligible with respect to much stronger spin interactions. Consequently, all the spins are directed in the x direction (the direction of the interaction, which is perpendicular to that of the magnetic field).

The change of $\left\langle \hat{I} \right\rangle^{gs}$ from zero to a positive value at λ_c happens continuously because $j\left(1-\frac{1}{\lambda_c}\right) = 0$. On the other hand, the first derivative $\frac{d}{d\lambda}\left\langle \hat{I} \right\rangle^{gs}$ has a jump discontinuity at λ_c from 0 to $j\lambda_c^{-2} = j$. Since a discontinuity in the l-th derivative of the order parameter is tied with an $(l+1)$th order QPT, we confirm that the QPT is second-order. All values related to the QPT are neatly reviewed in table 3.1.

Table 3.1: Order parameter values for the Lipkin Hamiltonian

	x^2_{min}	p^{gs}	E^{gs}	$\frac{d}{d\lambda}E^{gs}$	$\frac{d^2}{d\lambda^2}E^{gs}$	$\langle I\rangle^{gs}$	$\frac{d}{d\lambda}\left\langle \hat{I} \right\rangle^{gs}$
$\lambda < \lambda_c$	0	0	$-j$	0	0	0	0
$\lambda > \lambda_c$	$\frac{\lambda-1}{\lambda}$	0	$-j\left(1+\frac{(\lambda-1)^2}{2\lambda}\right)$	$\frac{j}{2}\left(\frac{1}{\lambda^2}-1\right)$	$-\frac{j}{\lambda^3}$	$j\frac{\lambda-1}{\lambda}$	$\frac{j}{\lambda^2}$
$\lambda \to \infty$	1	0	$-\infty$	$-\frac{j}{2}$	0	j	0

Excited-state quantum phase transition

The state with energy E_1 (as given in (3.21)) of a particle staying at x_1 does not cease to exist for $\lambda > \lambda_c$ but it turns into a local maximum energy (see fig. 3.1). It is a continuation of the sub-critical ground state. This potential maximum is responsible for the arisen ESQPT in the model. The particular ESQPT in the model is of type $(f, r) = (1, 1)$ and therefore connects to a logarithmic divergence of the smoothed density of states at the critical energy E_c. The critical energy in this model is independent of λ (apart from the fact that λ has to be greater than the critical value λ_c).

3.5 Parity conservation

The system has an inner symmetry which has an impact on the dynamics. It is better visible, when rewrite Hamiltonian (3.6) in terms of spin ladder operators

(3.9) and (3.10),

$$\begin{aligned}\hat{H} &= \hat{J}_0 + \lambda\left(-\frac{1}{2j}\left[\frac{\hat{J}_+ + \hat{J}_-}{2}\right]^2\right) = \\ &= \hat{J}_0 - \frac{\lambda}{8j}\left(\hat{J}_+^2 + \hat{J}_-^2 + \hat{J}_+\hat{J}_- + \hat{J}_-\hat{J}_+\right).\end{aligned} \tag{3.25}$$

Now we see, that all terms in (3.25) shift $\hat{J}_3$ eigenvalue either by 0 or ± 2. Therefore, it is possible to introduce parity

$$\hat{P} = (-1)^{\hat{J}_3 + j} \tag{3.26}$$

which is conserved during the evolution determined by Hamiltonian (3.6). The term $+j$ ensures that the exponent is an integer, since $\hat{J}_3$ has half-integer eigenvalues at the same time as j is a half-integer.

To profit from the parity conservation, we need to start with such initial state $|\psi(0)\rangle$ which has a well-defined parity, i.e. there are only even or only odd terms in the decomposition of $|\psi(0)\rangle$ into the standard basis $|j, m\rangle$ (where m represents a $\hat{J}_3$ eigenvalue).

Since $\hat{P}$ is conserved during the evolution determined by $\hat{H}(\lambda)$, it holds that $\left[\hat{P}, \hat{H}(\lambda)\right] = 0$. It follows that $\hat{P}$ and $\hat{H}(\lambda)$ are simultaneously diagonalizable and it is possible to choose such $\hat{H}(\lambda)$ eigenstates that have well-defined parity. The parity is conserved even if λ is being changed during the evolution because a sudden change of λ does not affect the $\hat{J}_3$ value.

For Hamiltonian (3.6), the parity can be expressed in terms of $\hat{H}_\mathrm{i}$ energy level number as $\hat{P} = (-1)^{k-1}$ (where $k = 1$ for the ground state). Which means we will consider only even-numbered energy levels. For $\lambda > \lambda_\mathrm{c}$, it follows from the fact that the eigenstates of a double-well potential form doublets of two energetically close states (see fig. 4.1). The same formula can be derived straightforwardly for $\lambda < \lambda_\mathrm{c}$. We obtained the coordinate-momentum representation by transforming boson operators $\hat{b}^\dagger$, $\hat{b}$ to $\sqrt{j}(x \pm ip)$ and so we can write also the particle number operator $\hat{b}^\dagger\hat{b}$ which returns the energy level number in a harmonic oscillator. From (3.11) we see that

$$\hat{P} = (-1)^{\hat{J}_3 + j} = (-1)^{\hat{b}^\dagger\hat{b}} = (-1)^{k-1} \tag{3.27}$$

because here we label energy levels starting from $k = 1$ and for the standard linear harmonic oscillator the ground state corresponds to the zeroth energy.

We will investigate the dynamics only for positive parity states. In other words, we will take exclusively odd-energy-level eigenstates of $\hat{H}_\mathrm{i}$ as the initial state $|\psi(0)\rangle$. The parity conservation signifies that there are no terms in the Hamiltonian which mediate an interaction between states of different parities. Therefore the proper Hilbert space in our case is the one that includes only positive-parity states. For that reason, we will consider only such basis states in the formulae for the Heisenberg time (2.22) and for the participation ratio (2.17).

4. Numerical results

QPTs occur in the infinite system size and so it is desired to perform all numerical computations for high j. On the other hand, we are limited by the program runtime. We used $j = 1000$ for all computations, if not specified otherwise. We provide a comparison of numerical results for different system sizes in appendix B. Briefly, the system behaves qualitatively correctly (for studying QPTs) for approximately $j > 30$. Smaller j-values result in distorted graphs and possibly in omitting a whole regime of the survival probability evolution.

4.1 Energy levels

A first insight into a quantum system can be get by knowing its eigenenergies. Let us begin with fig. 4.1 which shows how the eigenenergies of $\hat{H}(\lambda)$ change with varying λ. The spectrum of the plane $\lambda \times E$ of Hamiltonian (3.6) is scaled by j so we plot the quantity $\frac{E}{j}$ which is scale invariant. Only the number of eigenstates increases with higher j and the spectrum of $\frac{\hat{H}}{j}$ gets denser. Therefore we choose $j = 25$ for the sake of legibility. In the figure we see that the eigenstates change their structure and form doublets at the critical energy $E_c = -j$, as predicted in section 3.5. Figure 4.2 replots the eigenenergies dependency on control parameter λ for positive-parity eigenstates.

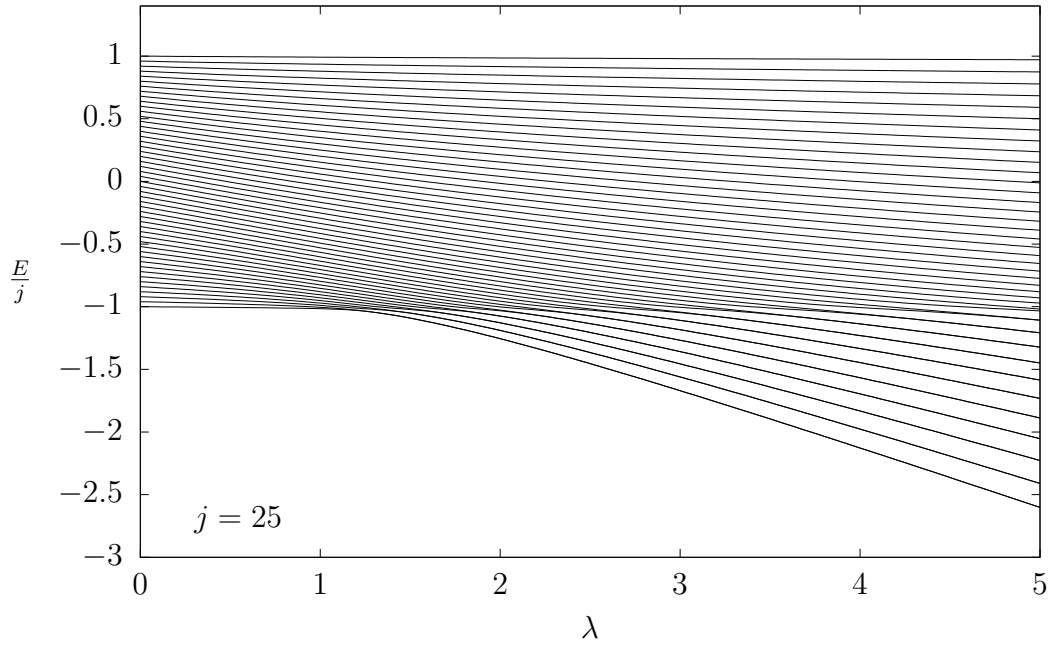

Figure 4.1: Dependency of both-parity $\hat{H}(\lambda)$ eigenvalues on λ

A vertical cross-section at a certain value of λ in fig. 4.2 represents the distribution of the initial state $|\psi(0)\rangle$ into the eigenstates of the corresponding Hamiltonian $\hat{H}(\lambda)$ which specifies the cross-section. State density ρ at (λ, E) can be visualized as the reciprocal vertical distance of two neighbouring levels. It is visible that the eigenstates cluster around the critical energy E_c for $\lambda > \lambda_c = 1$. All

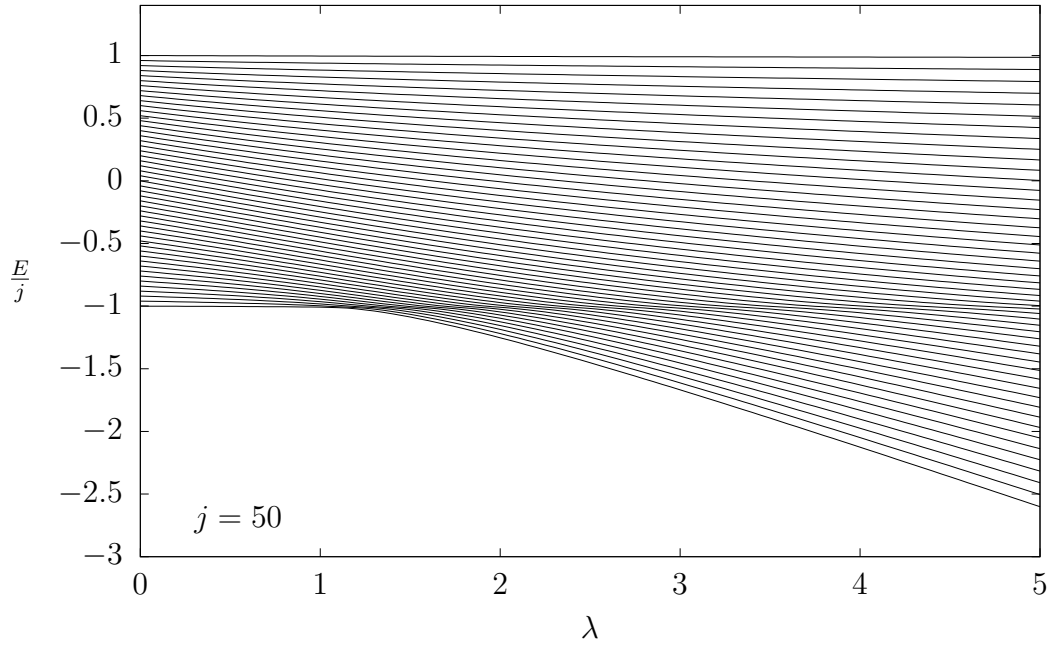

Figure 4.2: Dependency of positive-parity $\hat{H}(\lambda)$ eigenvalues on λ

the eigenstates turn at the critical energy and go horizontal for a while. In this manner, they create a divergence of the density of states caused by the ESQPT in the model.

4.2 Backward quench protocols

One possibility for a quench protocol is to start on the ground state above the critical point λ_c and to quench backwards. Figure 4.3 shows the survival probability and the corresponding strength function for three characteristic backward quench protocols (BQPs) which end in the phase below the ESQPT, above the ESQPT and on their borderline.

The initial decay is almost exactly Gaussian. Then the survival probability revives and after a series of approximately power modulated oscillations (depicted in the log-log scale as linear envelopes of the oscillations) the survival probability saturates and then fluctuates around the mean value $\mathcal{N}^{-1}$. The ESQPT accelerates the decay of the initial state (and its stabilization in the final Hamiltonian) in the critical quench by skipping the entire long-time regime.

From the three strength function graphs in fig. 4.3, one can see that the eigenstates are truly much closer in vicinity of E_c (notice different scales on the x axis!), exactly as expected from a precursor of the divergence in the density of states. Since all basis states (of one parity) are populated after a quench, it is easy to compare strength function graphs for the same class of quench protocols differing only in quench lengths $\Delta\lambda$.

The energy distribution is approximately Gaussian and the ESQPT suppresses the population of the critical-energy states.

A more compact perspective on how the survival probability changes with different quench lengths $\Delta\lambda$ can be get from a map plot at fig. 4.4. Apart from

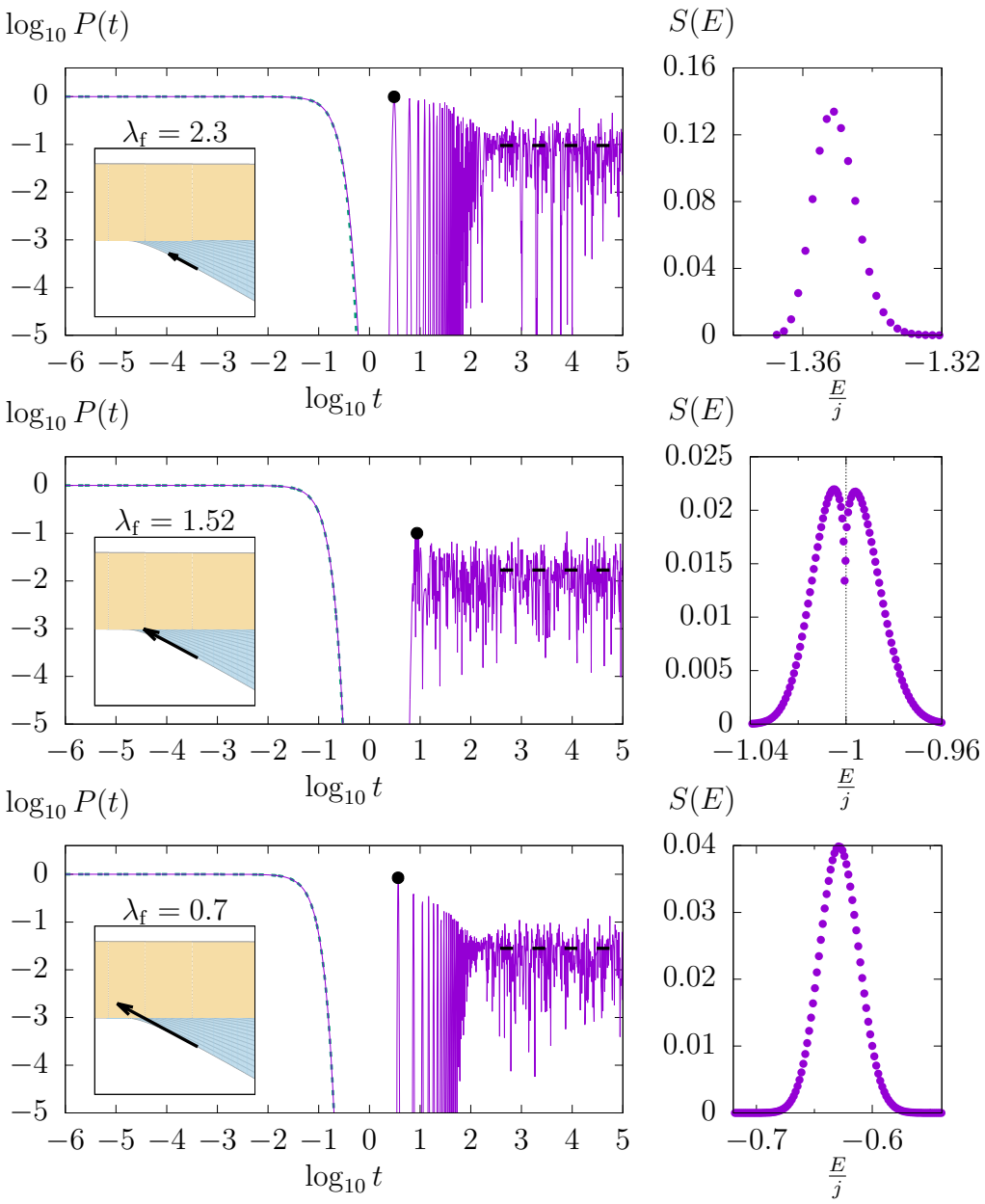

Figure 4.3: BQPs from the ground-level energy starting at $\lambda_i = 3.2$ and ending in the phases below and above the ESQPT and on their borderline. The insets indicate the course of each respective quench protocol (the shift in $\langle E_f \rangle_i$). The survival probability graphs incorporate an approximating Gaussian decay (thick dashed green line), the Heisenberg time (black bullet) and the long-time mean survival probability $\mathcal{N}^{-1}$ (thick black dashed line). Critical energy E_c is labelled in the strength function graphs (black dotted line).

the obvious fact the initial state decays slowly in similar Hamiltonians (for which $\Delta\lambda \sim 0$), we see that the for a general $\Delta\lambda$, it decays and ultimately stabilizes around a certain level with a few recurrences.

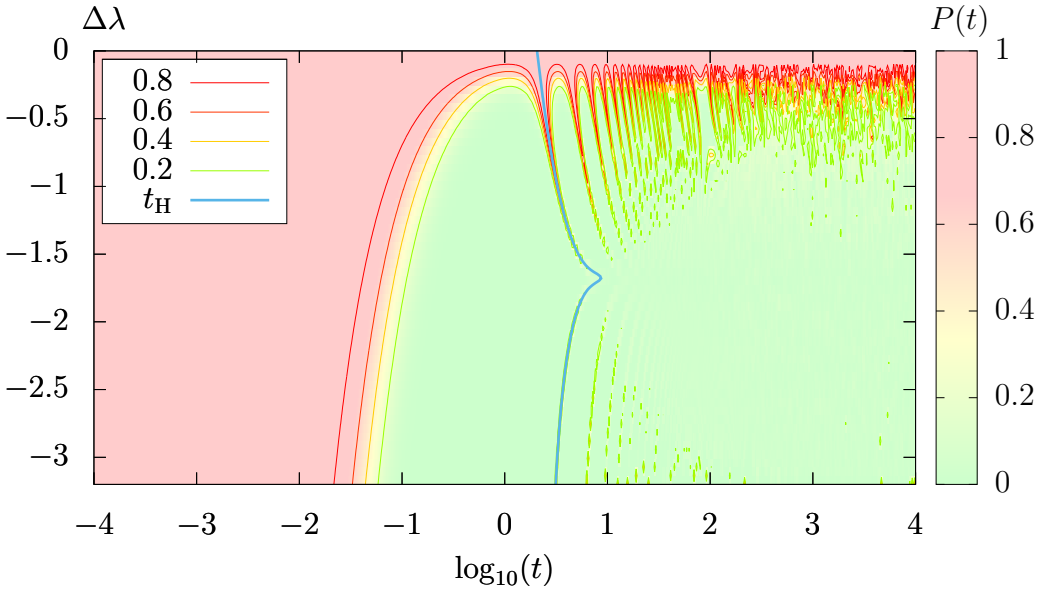

Figure 4.4: Survival probability for BQPs from the ground state at $\lambda_\mathrm{i} = 3.2$ as a function of the quench length $\Delta\lambda$ and time t. Critical quench length (the quench ends on the ESQPT borderline) is marked with a black dotted line and the Heisenberg time is marked with a thick blue line.

The Heisenberg time is in a perfect alignment with the first recurrence and it has a maximum at the critical quench length $\Delta\lambda_\mathrm{c}$ (for which the quench ends on the ESQPT borderline). Not only does the ESQPT skip the phase of modulated oscillations, it also prolongs the time before the first recurrence, which is weaker in this case (fig. 4.3), the saturation phase comes earlier.

The corresponding map plot of the strength function is in fig. 4.5. The support of $S(E)$ for each $\Delta\lambda$ is small with respect to the maximum energy difference in fig. 4.5. For that reason, there are no visible effects in the graph. The same graph for smaller system sizes is less localized and it clearly shows the suppression of near-critical energies (see fig. B.3). To make fig. 4.5 more telling, we could subtract the linear dependency as given by (2.20). Then. it would show the eigenstates structure, not just the trend.

We did not examine BQPs starting from excited-states because the effect both in the survival probability and the strength function are even weaker than for the ground-state BQPs. The reason is that excited states are notably delocalized over the energy spectrum.

Most of the these facts about the Heisenberg time, participation ratio and density of states also hold for all following quench protocols.

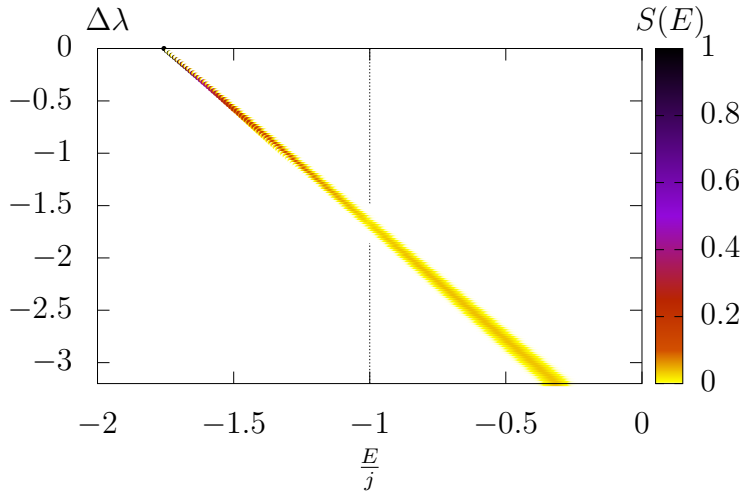

Figure 4.5: Strength function for BQPs from the ground state of $\lambda_\mathrm{i} = 3.2$ as a function of the quench length $\Delta\lambda$ and time t. Critical energy is marked with a black dotted line.

4.3 Forward quench protocols

Another possibility for a quench is to start under the critical point λ_c, say $\lambda_\mathrm{i} = 0$, and then to quench forwards, the so called forward quench protocol (FQP). We will denote the j-th or $(j-1)$th energy state (whichever has the correct parity) as the middle-energy level and $(2j)$th energy level as the maximum-energy level.

Ground state

Let us start with FQPs from the ground-state. As can be seen from table 3.1, the λ-derivative of the ground-state energy is zero, and therefore the quench will follow the separatrix. Characteristic quench protocols are shown in fig. 4.6.

The initial state has energy E_c and the mean energy $\langle E_\mathrm{f} \rangle_\mathrm{i}$ is also E_c for each λ. Thanks to the high density of states along the separatrix, it is easy to reconstruct the initial state with only a few $\hat{H}_\mathrm{f}$ eigenstates. This is reflected both in the strength function which has a sharp peak at E_c and in the survival probability which does not decay much (and that at a sub-Gaussian rate), then it stabilizes at a high value. In the classical correspondence it matches with a particle set in the minimum of a quadratic potential well, and the particle keeps steady during the process in which the minimum then turns into a maximum of a double-well potential.

Graphs 4.7 and 4.8 represent the evolution of the survival probability and the strength function throughout the gradually longer quenches. The ESQPT in this case stabilizes the initial state as both the initial decay and Heseinberg time are shifted at larger times. There is a lot of recurrences for all quench lengths $\Delta\lambda$ and those at $\Delta\lambda_\mathrm{c}$ are by far the highest of all. There are dense- and sparse-spectrum areas in fig. 4.8. The areas reflect the number of eigenstates in vicinity of E_c at λ_f. This detailed structure is observed only because of a different energy scale than on the rest of analogous graphs.

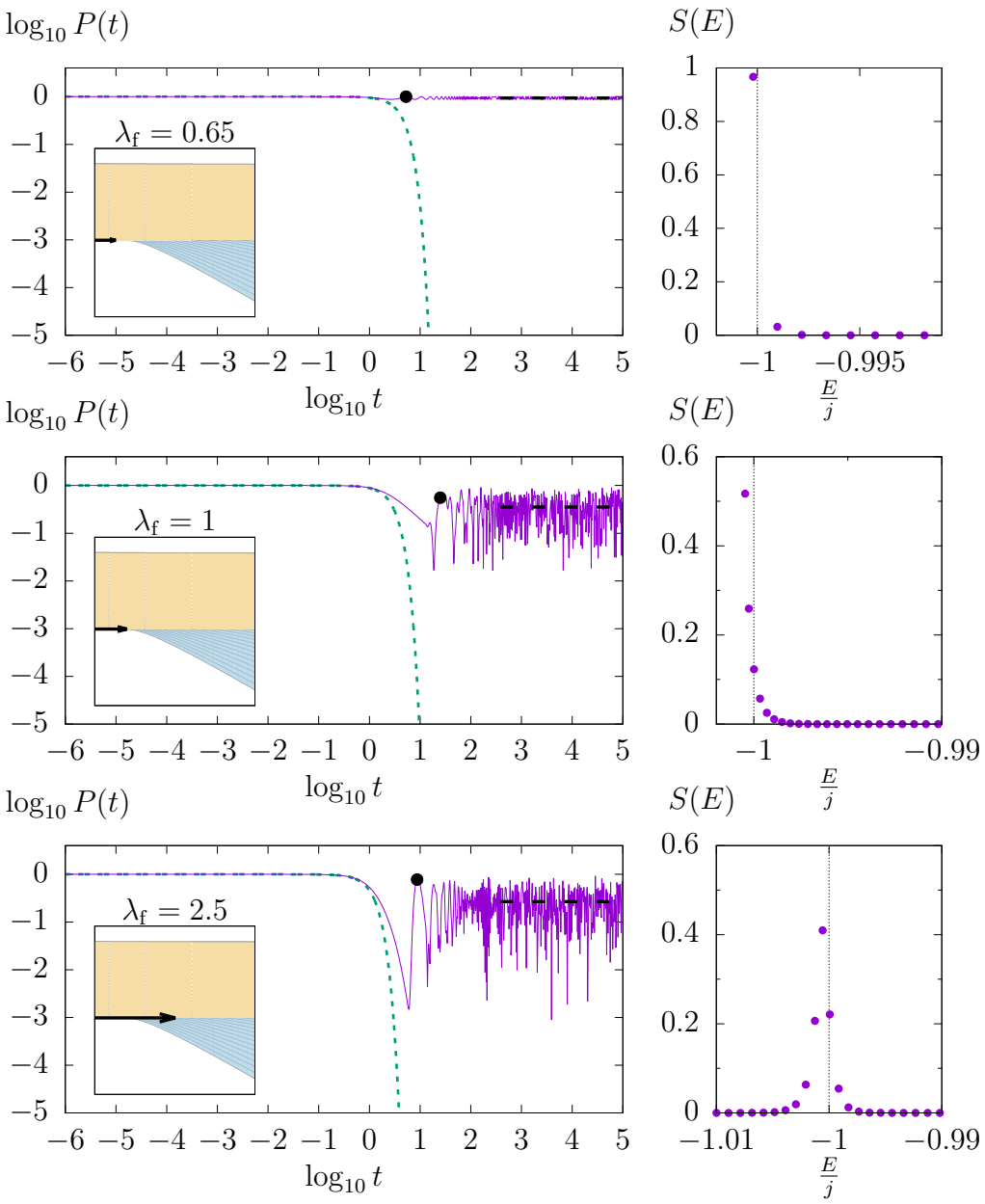

Figure 4.6: FQPs from the ground-level energy starting at $\lambda_\mathrm{i} = 0$ and ending in the phases below and above the ESQPT and on their borderline. The insets indicate the course of each respective quench protocol (the shift in $\langle E_\mathrm{f} \rangle_\mathrm{i}$). The survival probability graphs incorporate an approximating Gaussian decay (thick dashed green line), the Heisenberg time (black bullet) and the long-time mean survival probability $\mathcal{N}^{-1}$ (thick black dashed line). Critical energy E_c is labelled in the strength function graphs (black dotted line).

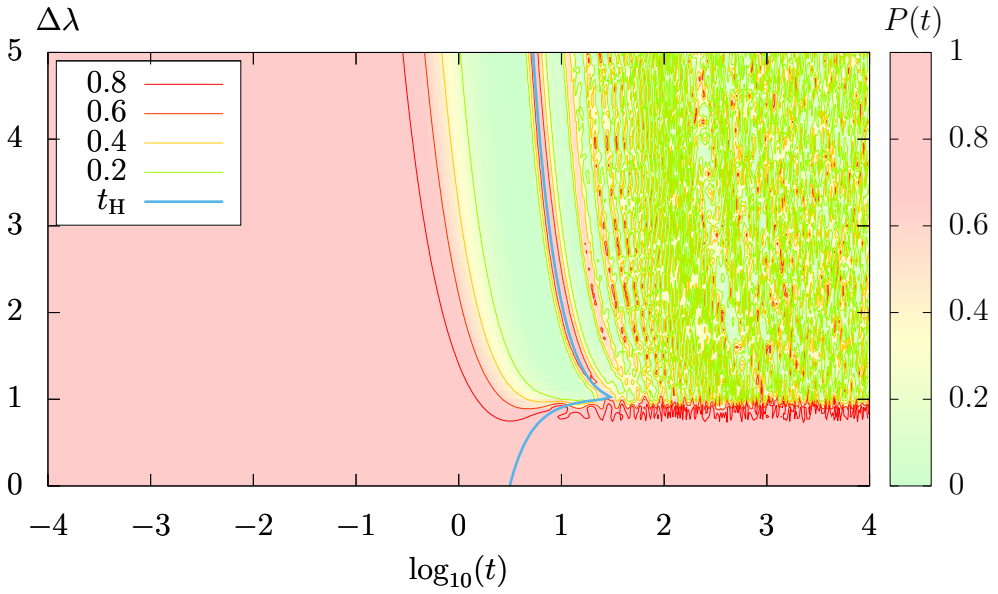

Figure 4.7: Survival probability for FQPs from the the ground of $\lambda_{\mathrm{i}} = 0$ as a function of the quench length $\Delta\lambda$ and time t. Critical quench length (the quench ends on the ESQPT borderline) is marked with a black dotted line and the Heisenberg time is marked with a thick blue line.

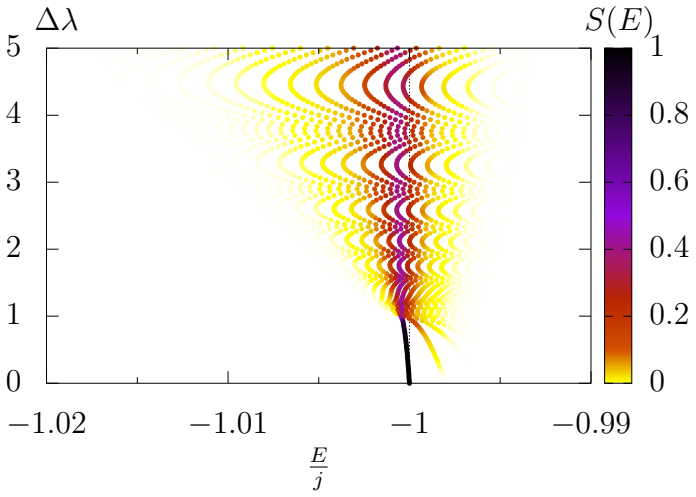

Figure 4.8: Strength function for FQPs from the ground of $\lambda_{\mathrm{i}} = 0$ as a function of the quench length $\Delta\lambda$ and time t. Critical energy is marked with a black dotted line.

Middle-energy state

The next option is to begin with the middle-energy state. A few quenches are shown in fig. 4.9 and the whole picture is in fig. 4.10 and fig. 4.11. A forward quench from the middle of the initial spectrum totally disrupts the initial state, making it decay earlier and deeper. There are even no recurrences in fig. 4.10. The initial decay (which is faster than Gaussian) smoothly follows in modulated oscillations. The Heisenberg time is at the end of the modulated oscillations phase, contrary to all the other quench protocols. After t_{H} the survival probability stays saturated approximately at that level.

Excited-states are highly delocalized over the energy spectrum, and consequently, the effect given by the ESQPT is less apparent. The classical intuition is that excited-states in a harmonic oscillator are delocalized in space. The correspondence with a particle in a potential well does not hold for the maximum energy state, because the spectrum of a potential well is infinite. Therefore it does not violate the intuition.

The strength function has two major peaks at the end of the populated spectrum. The distance between the peaks increases as $\Delta\lambda$ and the energy variance grow. For more detailed structure of the strength function see the strength function for $j = 60$ in fig. B.9. The energies around E_{c} are in these protocols inhibited again, however, the effect is minor in this case. Because of that, the survival probability does not change much with different quench lengths $\Delta\lambda$. Nevertheless, the initial decay comes earlier for larger quench lengths. Another tiny quantitative difference can be seen in the survival probability as one peak reaches the critical energy – the long-time average decreases. At this point, the Heisenberg time changes its trend and begins to decrease even faster.

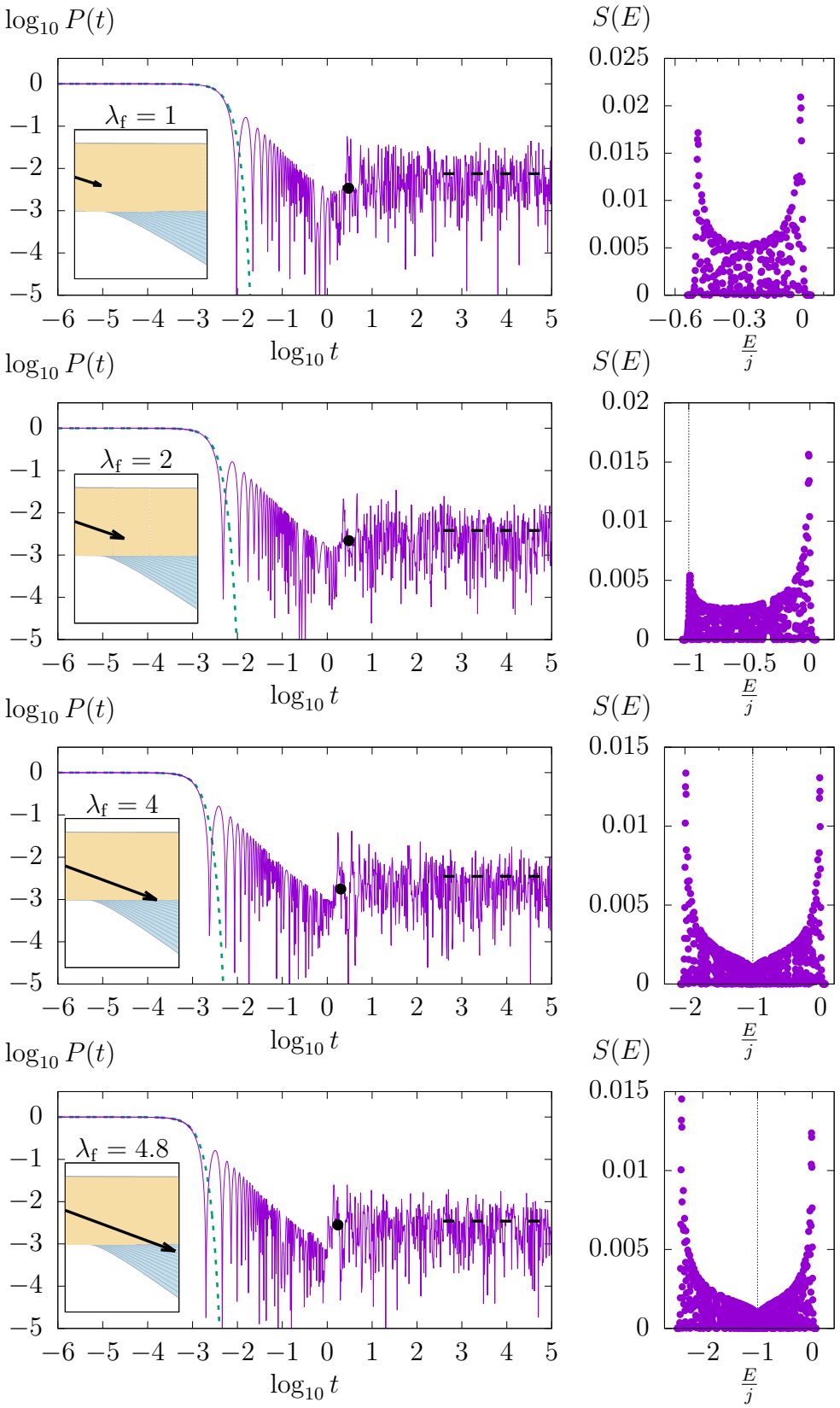

Figure 4.9: FQPs from the middle-level energy starting at $\lambda_i = 0$. The insets indicate the course of each respective quench protocol (the shift in $\langle E_f \rangle_i$). The survival probability graphs incorporate an approximating Gaussian decay (thick dashed green line), the Heisenberg time (black bullet) and the long-time mean survival probability $\mathcal{N}^{-1}$ (thick black dashed line). Critical energy E_c is labelled in the strength function graphs (black dotted line).

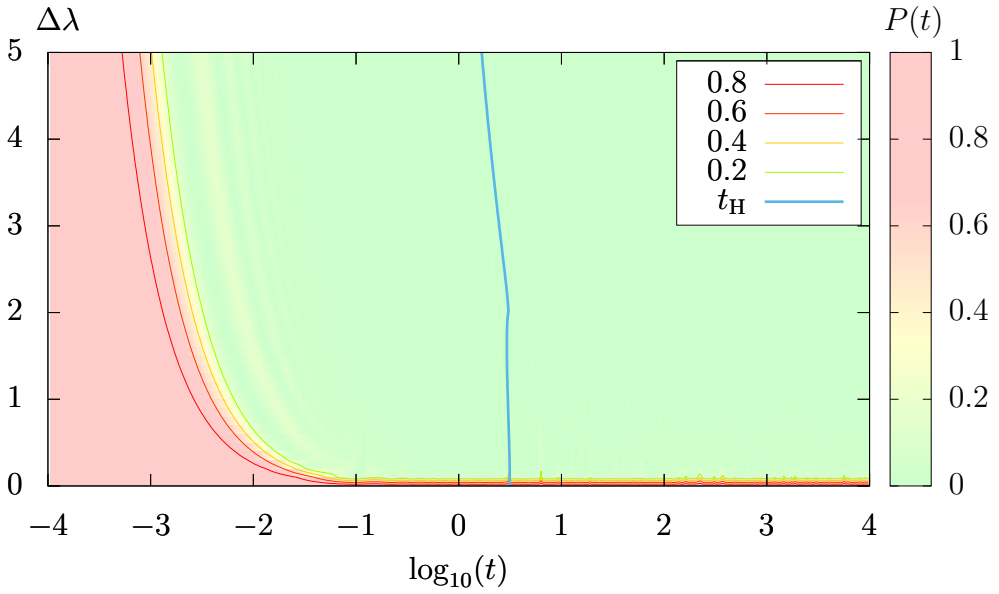

Figure 4.10: Survival probability for FQPs from the middle-energy at $\lambda_i = 0$ as a function of the quench length $\Delta\lambda$ and time t. Critical quench length (the quench ends on the ESQPT borderline) is marked with a black dotted line and the Heisenberg time is marked with a thick blue line.

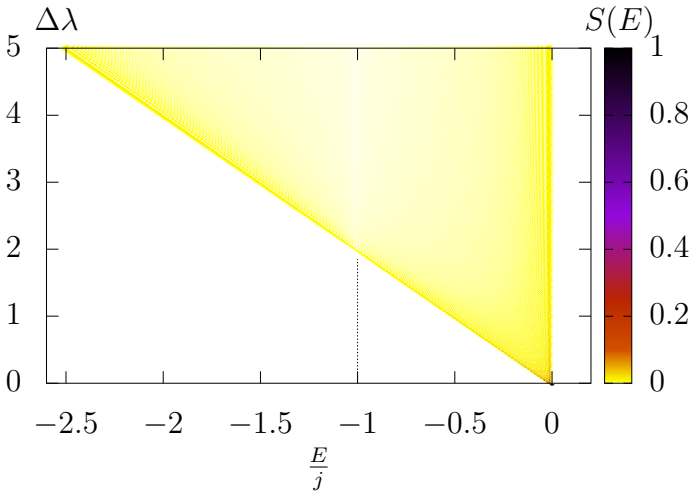

Figure 4.11: Strength function for FQPs from the middle-energy at $\lambda_i = 0$ as a function of the quench length $\Delta\lambda$ and time t. Critical energy is marked with a black dotted line.

Maximum-energy state

The last investigated FQP begins at the maximum-energy state which has immensely small λ-derivative. Therefore it will not cross the ESQPT borderline until $\log_{10} t = 8000$. We can safely assume that the tangent is horizontal and the quench will always stay in the phase above ESQPT. Figures 4.12, 4.14 and 4.13 show that the initial state remains highly localized – the survival probability does not decay and the strength function has a sharp peak at $\frac{E}{j} = 1$. The Heisenberg time still aligns with the first recurrence peak (contour 0.8 in fig. 4.13 marks depressions unlike on the rest of the graphs where contours mark peaks).

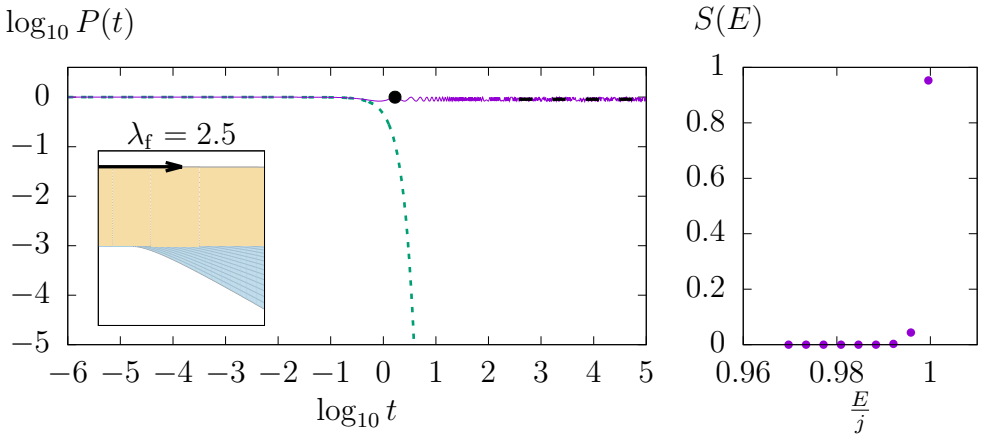

Figure 4.12: FQP from the maximum-level energy starting at $\lambda_\mathrm{i} = 0$ and ending in the phase above the ESQPT. The inset indicates the course of the quench protocol (the shift in $\langle E_\mathrm{f} \rangle_\mathrm{i}$). The survival probability graph incorporates an approximating Gaussian decay (thick dashed green line), the Heisenberg time (black bullet) and the long-time mean survival probability $\mathcal{N}^{-1}$ (thick black dashed line). Critical energy E_c is labelled in the strength function graphs (black dotted line).

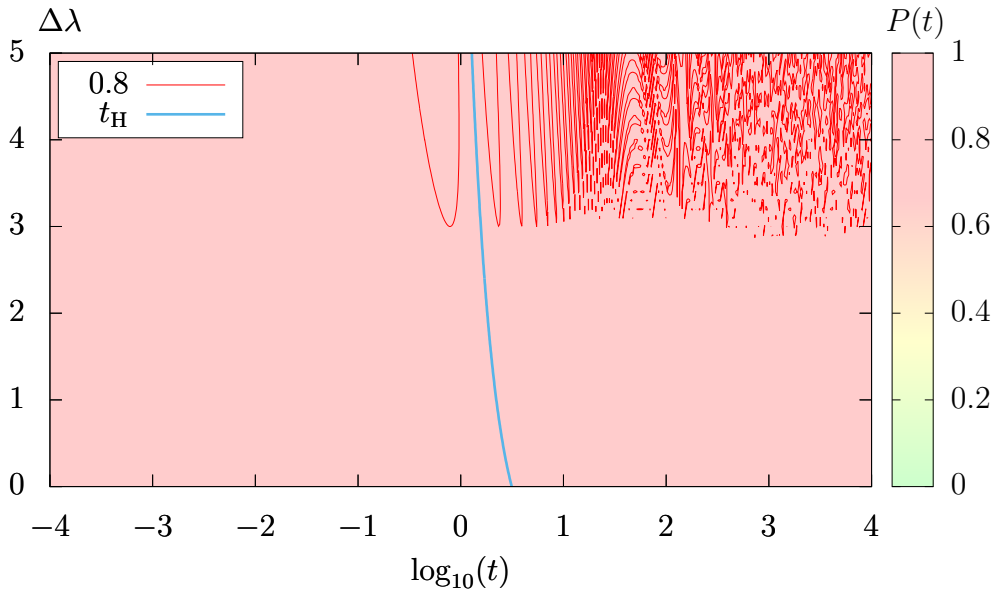

Figure 4.13: Survival probability for FQPs from the maximum-energy state starting at $\lambda_i = 0$ as a function of the quench length $\Delta\lambda$ and time t. The critical quench length $\Delta\lambda = 8000$- The Heisenberg time is marked with a thick blue line.

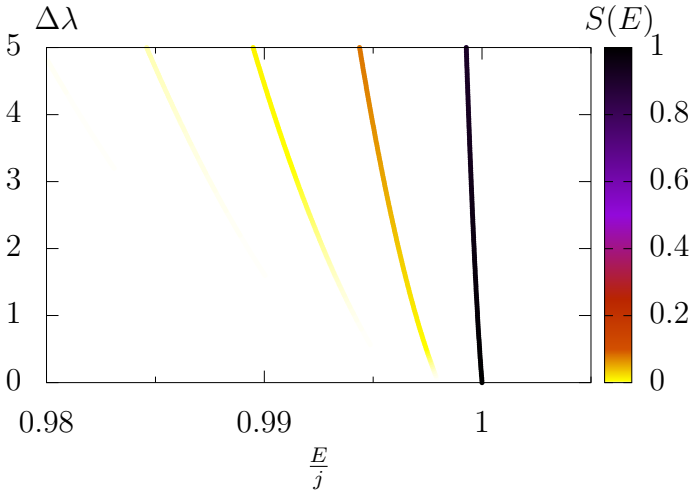

Figure 4.14: Strength function for FQPs from the maximum-energy state starting at $\lambda_i = 0$ as a function of the quench length $\Delta\lambda$ and time t. Critical energy $E_c/j = -1$.

Conclusion

We computed the survival probability and the strength function for ground-state BQPs and for ground-state, middle-energy and maximum-energy FQPs. First, we verified that the initial state decays according to the scheme presented in chapter 2 and that the Heisenberg time lies either at the beginning or at the end of the modulated oscillations stage, and that the inverse of the participation ratio predicts well the long-time mean survival probability. We noticed that the density of states is significantly higher in vicinity of the critical ESQPT energy.

The initial state in a ground-state BQP decays and then exhibits plenty of recurrences. If the endpoint of the quench lies on the critical energy, the state decays more quickly and the following recurrences are suppressed. The strength function is approximately Gaussian. The critical-energy states are suppressed.

In a ground-state FQP, the initial state does not decay much and a high fraction of the initial state stays present and keeps reappearing in the following oscillations. The critical-length quench stabilizes the initial state which then decays more slowly. The strength function is a sharp peak at the initial energy which is equal to the critical energy.

A middle-state FQP makes the initial state decay very quickly and suppresses all the following recurrences. The critical quench is not different from non-critical quenches because the initial excited state has high energy variance and therefore lies in both phases at once. The strength function has a U-shape whose lower-energy edge is shifted even lower for large quench lengths. The states with the critical energy are slightly suppressed.

In the Lipkin model, a maximum-energy FQP corresponds to a shift along a constant eigenenergy. Hence, the initial state decays minimally (and probably due to the finite dimension). The strength function is a sharp peak at the initial energy which does not overlap with the critical energy.

All in all, the effect of an ESQPT on the quench dynamics is not even qualitatively universal. Even though the same information is concealed in the Loschmidt amplitude as in the strength function, the effect is always visible in the strength function and is not necessarily apparent in the survival probability.

Possible extensions to the thesis

Some deeper insight into the effect of an ESQPT on the survival probability and on the equilibration of a general initial state could be acquired from a few more graphs than we plotted. The Heisenberg time t_{H} and the long-time mean survival probability $\bar{P}(t)$ characterize the evolution. Based on the fact that quenching along the separatrix had completely different effect than quenching across the separatrix, the angle between the separatrix and the direction of the quench might play a decisive part. The angle is in this case equivalent to $\left.\frac{\mathrm{d}E}{\mathrm{d}\lambda}\right|_{\lambda_{\mathrm{i}}=0}$. The dependency on the approaching angle might have two different ways of realizing it – either from the same λ_{i} or so that $\Delta\lambda$ is equal for all quenches. Then, there was a difference between ground-state BQPs and middle-energy FQPs given by a different level of localization of the initial state. Therefore another input values which might play a part are, e.g. higher moments of the final Hamiltonian $\hat{H}_{\mathrm{f}}$ in the initial eigenstates or the participation ratio. We already confirmed in

chapter 2 that $\bar{P}(t) = \mathcal{N}^{-1}$. It might prove relevant, to compute all the other dependencies of t_{H} and $\bar{P}(t)$ on each of the approaching angle, higher moments of $\hat{H}_{\mathrm{f}}$ and $\mathcal{N}$. Thus, we would also find the level of correlation between t_{H} and $\bar{P}(t)$.

Mean values of different observables are classically accessible. In the Lipkin model, the only reasonable observable is the magnetization (sum of the constituent spin values times the probability of the corresponding spin being in that state). One more factor complicates things – the temperature. It causes random fluctuations and, consequently, also induces a distribution for the states of the spins. Therefore, investigating the magnetization of the spin lattice with respect to λ_{i}, λ_{f} and temperature will result in macroscopic phenomena which might find use, e.g. in research or possibly in medicine.

A. No-crossing theorem

To demonstrate the rarity of real energy level crossings, we will review in detail the reasoning in [10]. Let us have a Hamiltonian $\hat{H}(\lambda)$ depending on a single control parameter λ. Let us define the characteristic polynomial $\mathfrak{p}(\lambda, E)$ for Hamiltonian $\hat{H}(\lambda)$,

$$\mathfrak{p}(\lambda, E) = \det\left(\hat{H}(\lambda) - E\hat{\mathbb{I}}\right), \tag{A.1}$$

where $\hat{\mathbb{I}}$ is the identity operator. The definition of eigenenergy E is written as

$$\mathfrak{p}(\lambda, E) = 0\,. \tag{A.2}$$

By solving equation (A.2) we get a set of roots $E^{(k)}(\lambda)$ where k goes from 0 up to the system dimension N. Suppose that $E^{(1)}(\lambda)$ and $E^{(2)}(\lambda)$ undergo a real crossing at $\lambda = \lambda_0$. Let E_0 be the energy of the crossing, i.e. $E_0 = E^{(1)}(\lambda_0) = E^{(2)}(\lambda_0)$. Since we investigate energy level crossings, we suppose that $E^{(1)}(\lambda) \neq E^{(2)}(\lambda)$ in a deleted neighbourhood of λ_0.

Because we deal with energy level crossing, we know that E_0 is a double root of $\mathfrak{p}(\lambda_0, E)$. That implies

$$\mathfrak{p}(\lambda_0, E_0) = 0\,, \tag{A.3}$$

$$\frac{\partial \mathfrak{p}}{\partial E}(\lambda_0, E_0) = 0\,. \tag{A.4}$$

Equality (A.2) has to hold for each λ along any energy level $E^{(k)}(\lambda)$, in particular for $i \in \{1, 2\}$ and $\lambda = \lambda_0 + \delta\lambda$ close to λ_0,

$$\begin{aligned} 0 = \mathfrak{p}\Big(\lambda, E^{(k)}(\lambda)\Big) \approx \\ \approx \underbrace{\mathfrak{p}(\lambda_0, E_0)}_{0} + \frac{\mathrm{d}}{\mathrm{d}\lambda}\Big[\mathfrak{p}\Big(\lambda, E^{(k)}(\lambda)\Big)\Big]\Big|_{\lambda_0, E_0} \delta\lambda = \\ = \left(\frac{\partial \mathfrak{p}}{\partial \lambda}(\lambda_0, E_0) + \underbrace{\frac{\partial \mathfrak{p}}{\partial E}(\lambda_0, E_0)}_{0} \frac{\mathrm{d}E^{(k)}}{\mathrm{d}\lambda}(\lambda_0)\right)\delta\lambda = \\ = \frac{\partial \mathfrak{p}}{\partial \lambda}(\lambda_0, E_0)\delta\lambda\,. \end{aligned} \tag{A.5}$$

Thus, we obtained another condition for a real energy crossing,

$$\frac{\partial \mathfrak{p}}{\partial \lambda}(\lambda_0, E_0) = 0\,. \tag{A.6}$$

Equations (A.4) and (A.6) are independent. Therefore, for a real crossing to occur, two independent conditions have to be satisfied by varying a single control parameter λ. This, in general, happens very rarely (the Hamiltonian would have to be of a very special form). Real energy level crossings can appear in systems with a Hamiltonian which depends on at least two different control parameters.

B. Small system size

In this chapter, we present the same graphs for $j = 60$ as in the main text for $j = 1000$. Then, we show a selection of graphs for $j = 5$. We include a graph of eigenenergies for $j = 5$ to compare it with fig. 4.2 where $j = 50$. Before comparing graphs of the strength function, look twice for different energy scales!

A system with too small a size has only a few eigenstates. Consequently, the dynamics is rather different from that in an infinite-size system with a genuine quantum phase transition. For very small sizes, all quench protocols look alike and the maximum of the Heisenberg time does not align with the critical quench length, anymore (see section B.3). Because of the lack of eigenstates, the strength function loses it complex structure for small j.

The density of states in vicinity of the critical energy grows for increasing j (compare fig. 4.3 and fig. B.1). Therefore, the Heisenberg time for critical-length quench protocols increases, as well (compare fig. 4.3, 4.9 with fig. B.1, B.7). Apart from its maximum, the Heisenberg time does not change with different system sizes. The Heisenberg time is given by the spacing of energy levels which also remains the same (new levels are add the top, not in the middle of the spectrum).

For large sizes, recurrences of the initial state in the survival probability diminish. Depending on the quench protocol, also the initial decay might be accelerated. Particularly it depends on the value of $\left\langle\!\left\langle \hat{V}^2 \right\rangle\!\right\rangle_{\mathrm{i}}$ which determines the speed of the initial decay. Since the Heisenberg time remains the same, the gap between the initial decay and the first recurrence of the initial state (at the Heisenberg time) extends.

B.1 Backward quench protocols

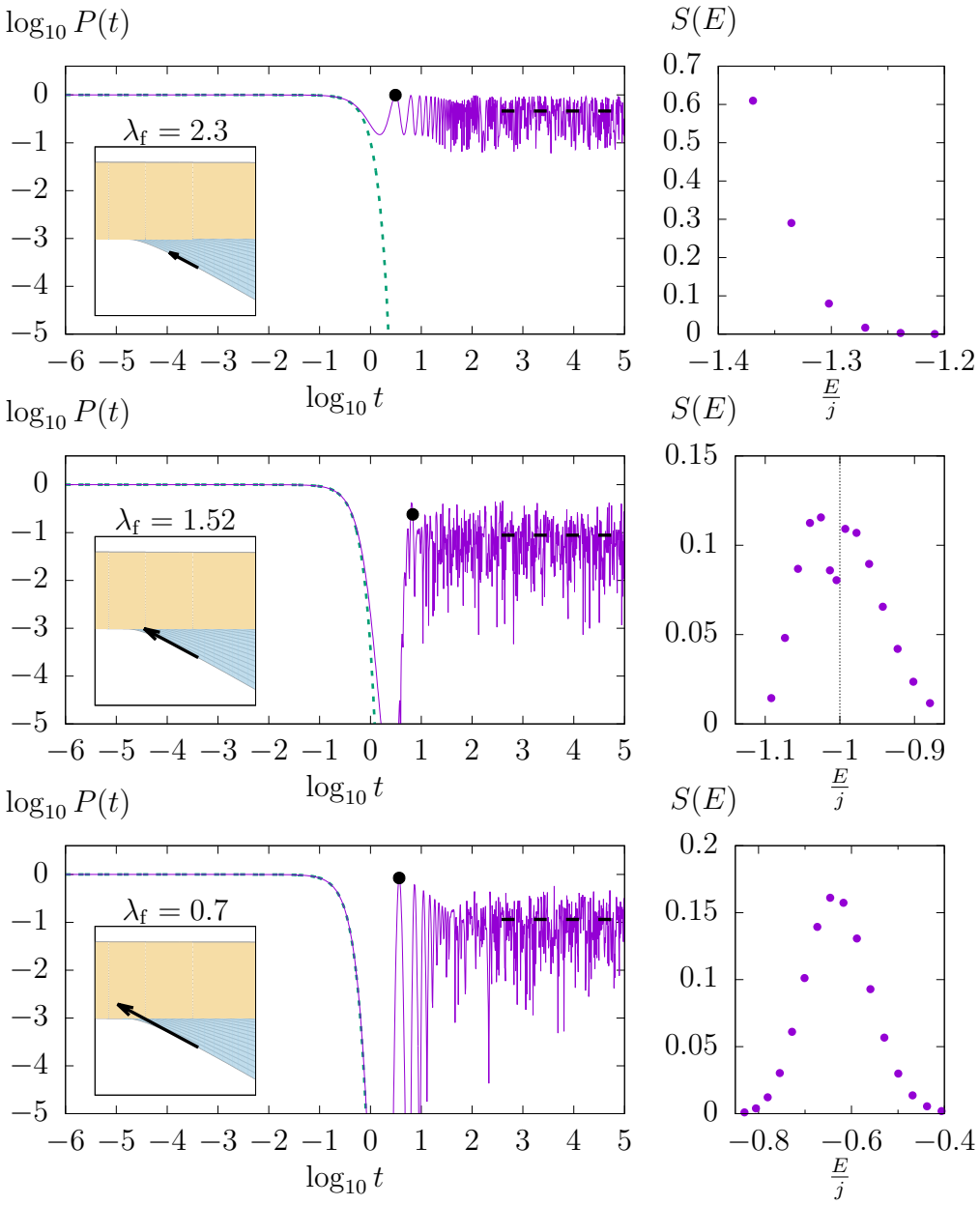

Figure B.1: BQPs from ground-level energy and $\lambda_i = 3.2$ ($j = 60$)

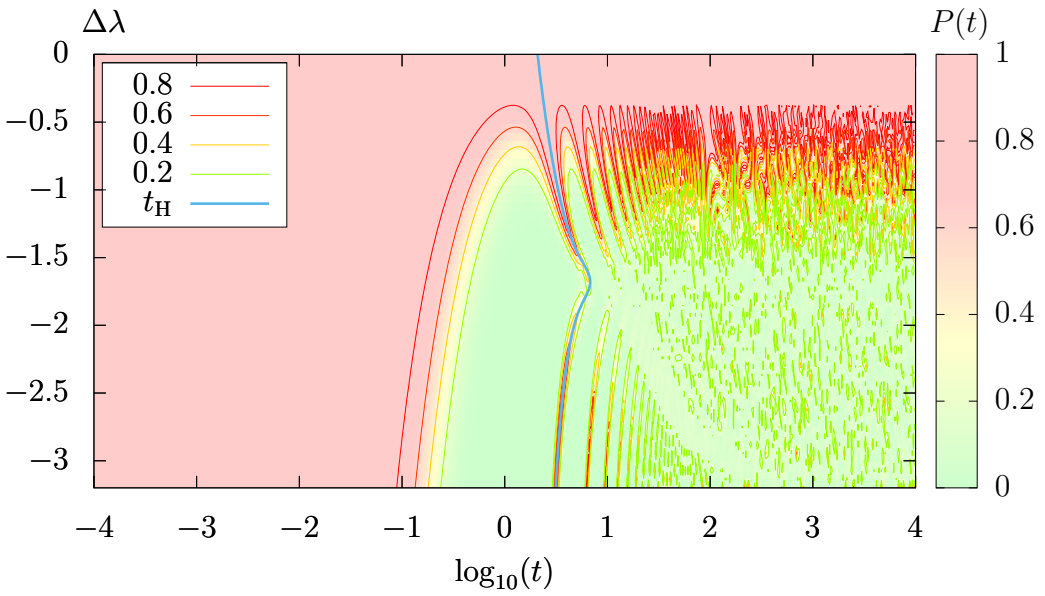

Figure B.2: Survival probability for BQPs from the ground state starting at $\lambda_i = 3.2$ as a function of the quench length $\Delta\lambda$ and time t ($j = 60$).

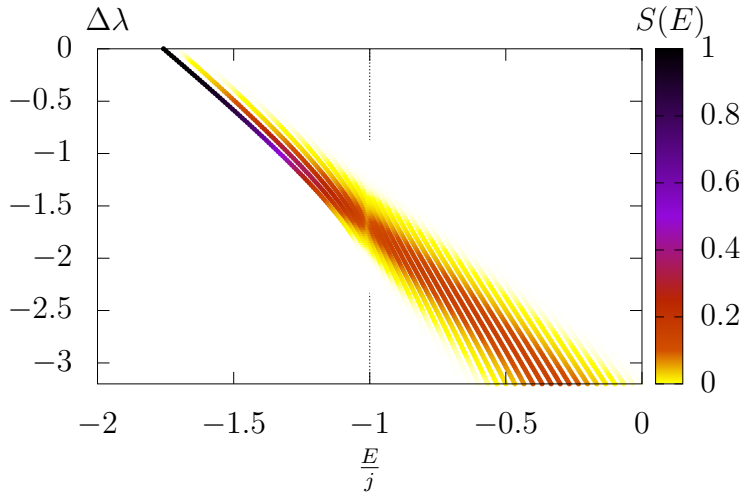

Figure B.3: Strength function for BQPs from the ground state at $\lambda_i = 3.2$ as a function of the quench length $\Delta\lambda$ and time t ($j = 60$).

B.2 Forward quench protocols

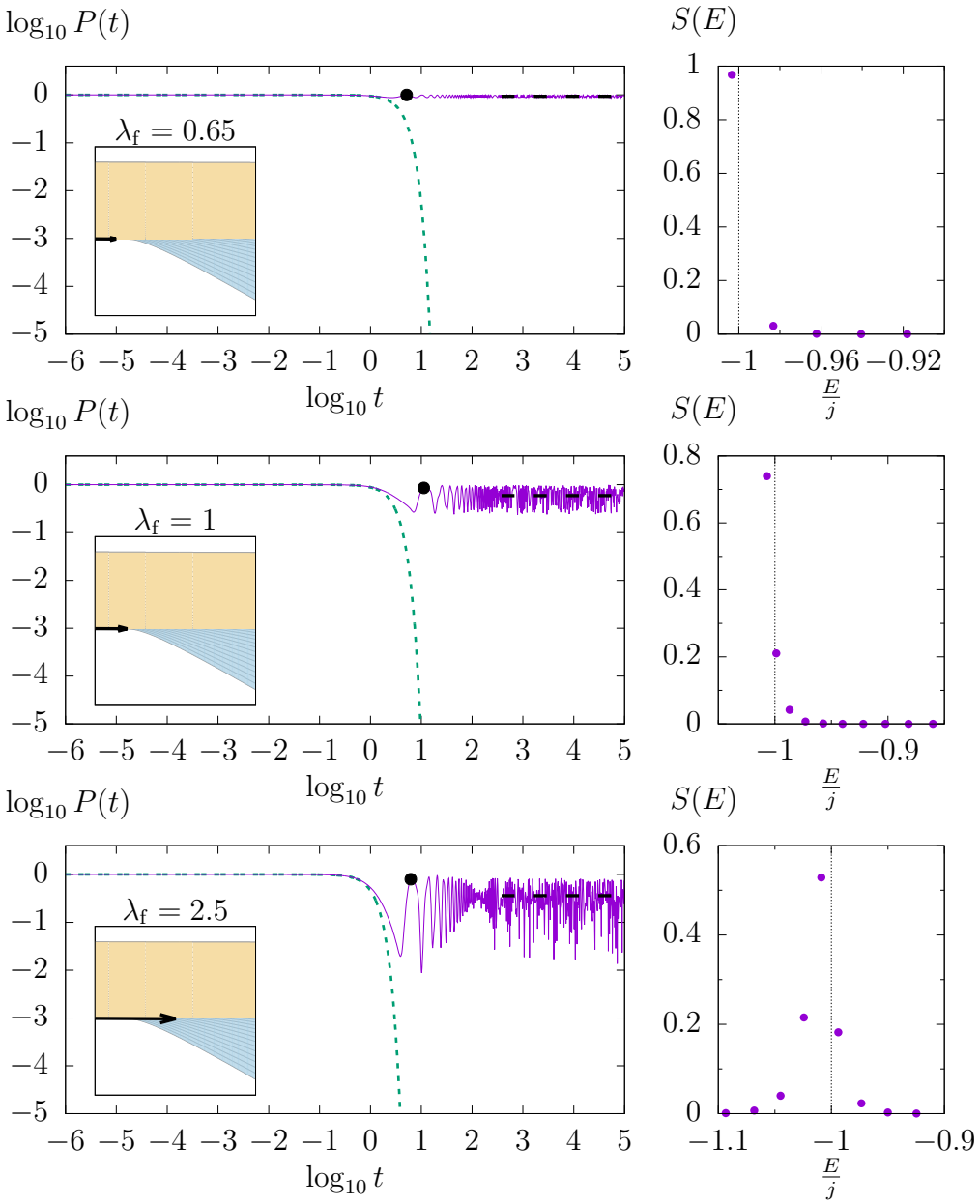

Figure B.4: FQPs from ground-level energy and $\lambda_i = 0$ ($j = 60$)

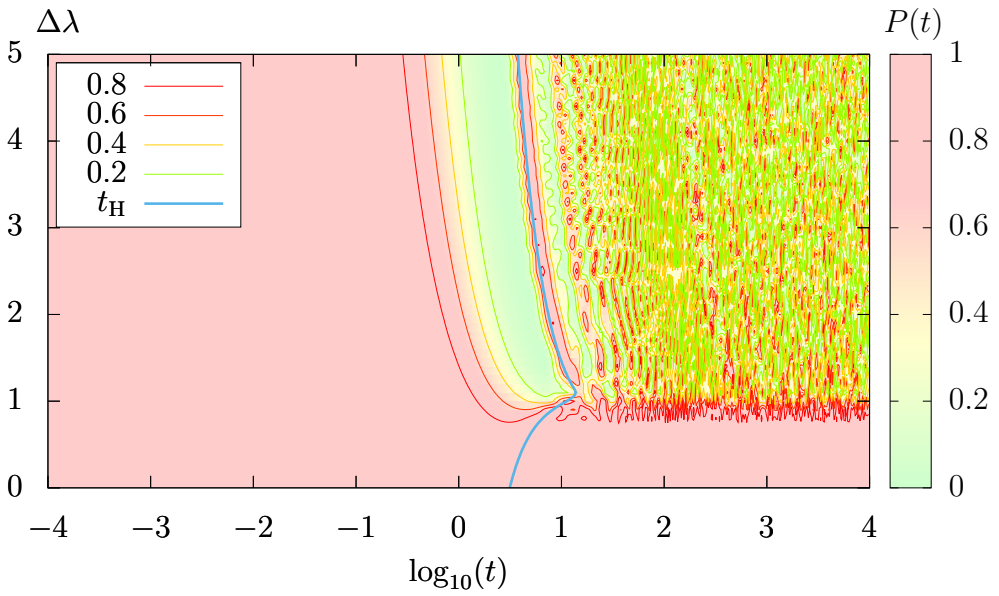

Figure B.5: Survival probability for FQPs from the ground state of $\lambda_\mathrm{i} = 0$ as a function of the quench length $\Delta\lambda$ and time t ($j = 60$).

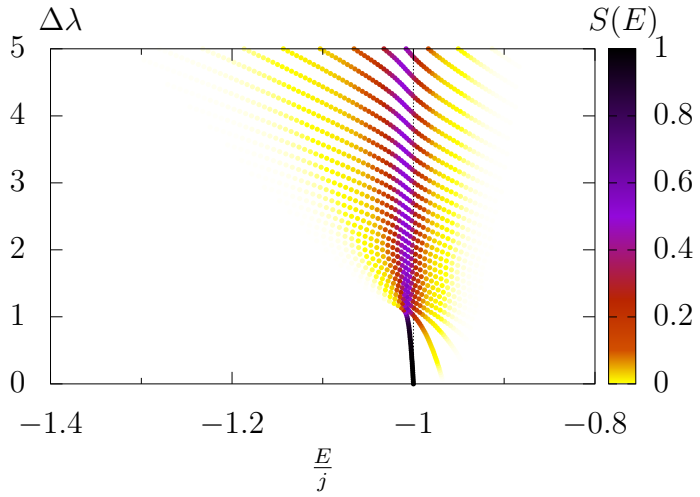

Figure B.6: Strength function for ground-state FQPs from $\lambda_\mathrm{i} = 0$ as a function of the quench length $\Delta\lambda$ and time t ($j = 60$).

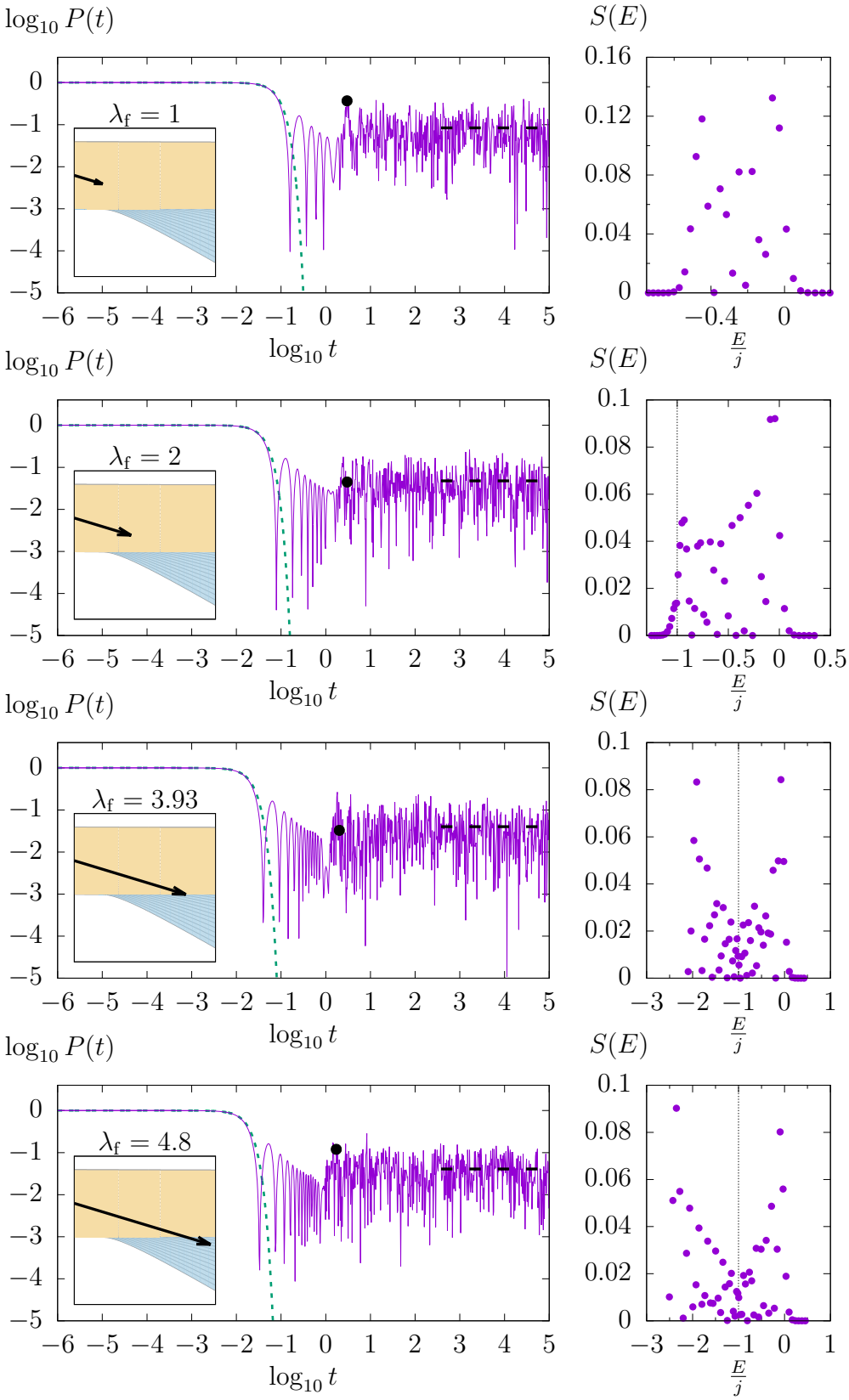

Figure B.7: FQPs from middle-level energy and $\lambda_i = 0$ ($j = 60$)

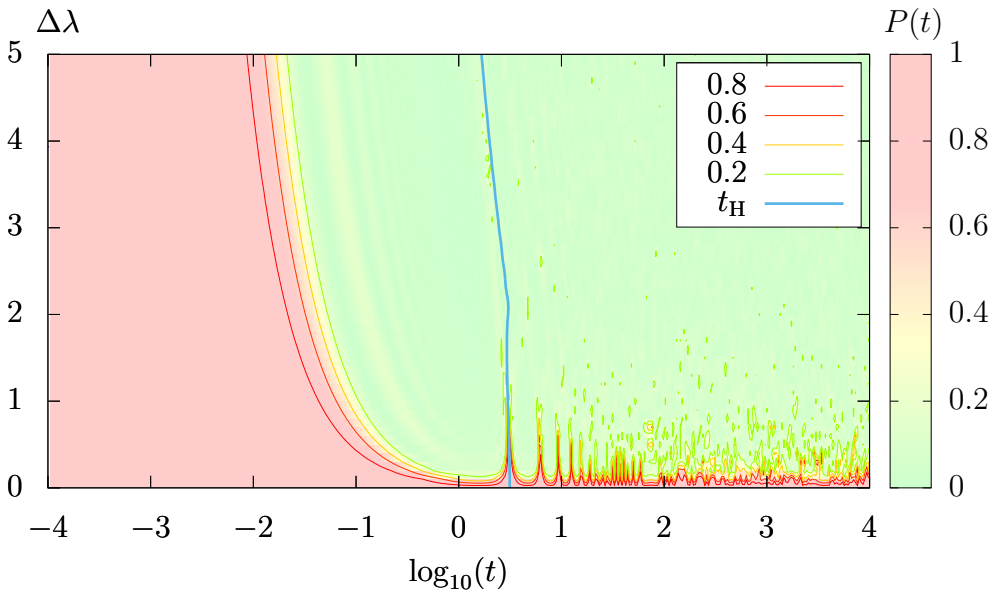

Figure B.8: Survival probability for FQPs from the middle-energy state of $\lambda_{\mathrm{i}} = 0$ as a function of the quench length $\Delta\lambda$ and time t ($j = 60$).

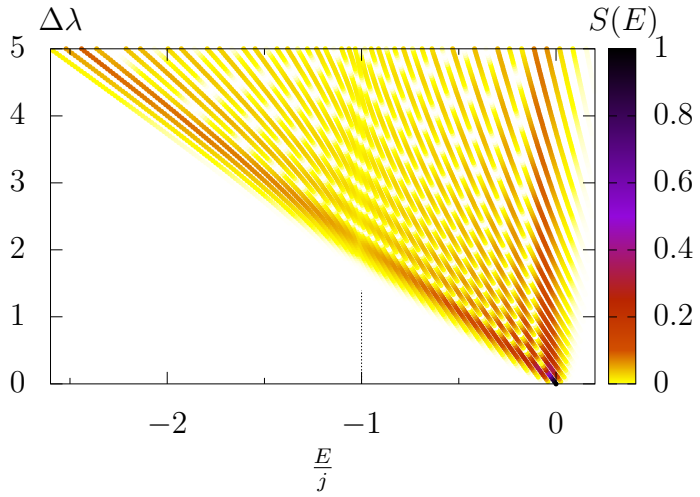

Figure B.9: Strength function for FQPs from the middle-energy state starting at $\lambda_{\mathrm{i}} = 0$ as a function of the quench length $\Delta\lambda$ and time t ($j = 60$).

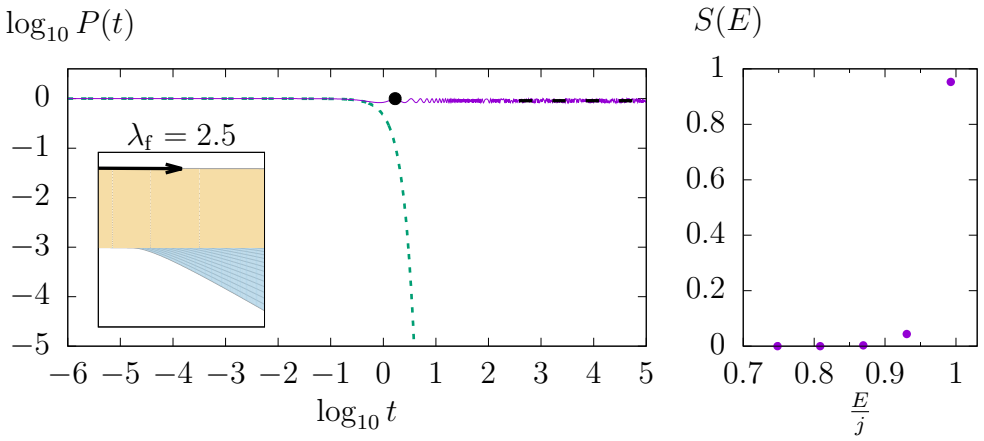

Figure B.10: FQP from maximum-level energy and $\lambda_i = 0$ ($j = 60$)

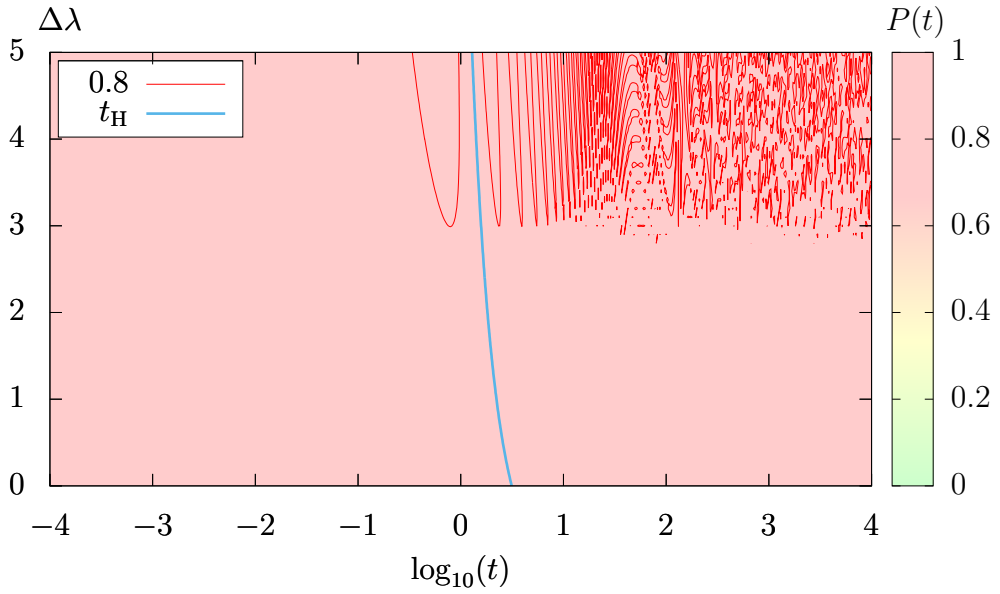

Figure B.11: Survival probability for FQPs from the maximum-energy state at $\lambda_i = 0$ as a function of the quench length $\Delta\lambda$ and time t ($j = 60$).

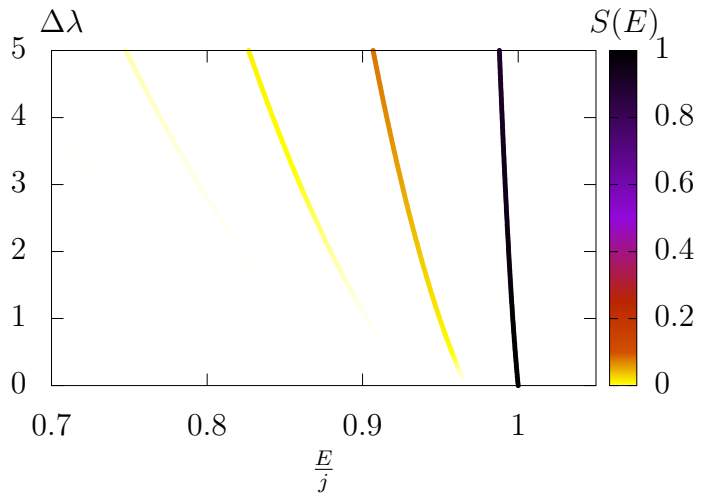

Figure B.12: Strength function for FQPs from the maximum-energy state starting from $\lambda_\mathrm{i} = 0$ as a function of the quench length $\Delta\lambda$ and time t ($j = 60$).

B.3 Very small system size

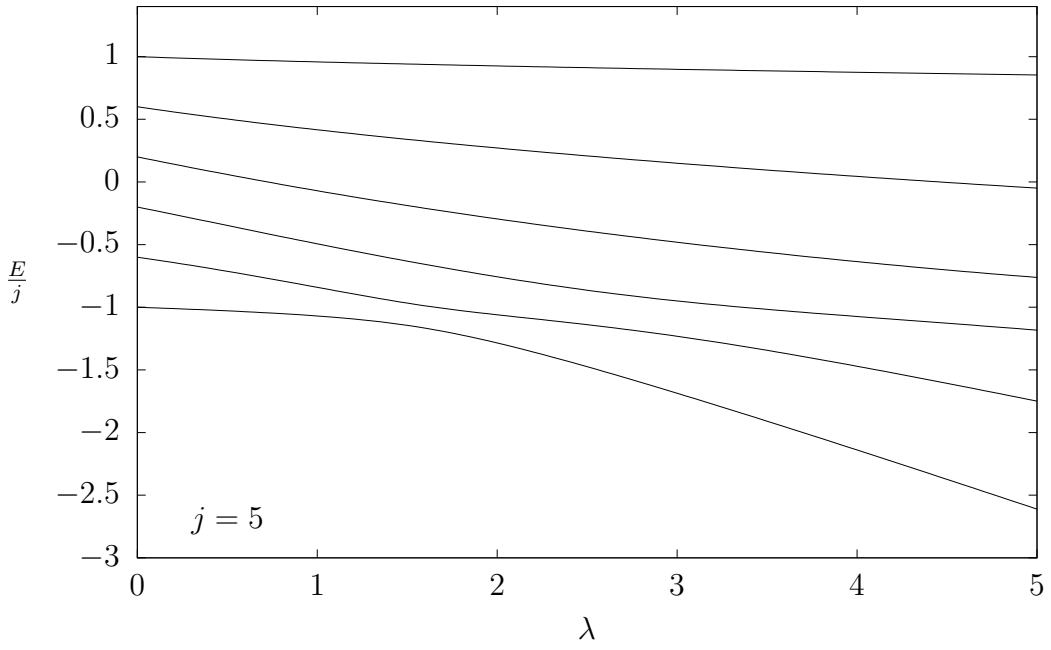

Figure B.13: Dependency of positive-parity $\hat{H}$ eigenvalues on λ ($j = 5$)

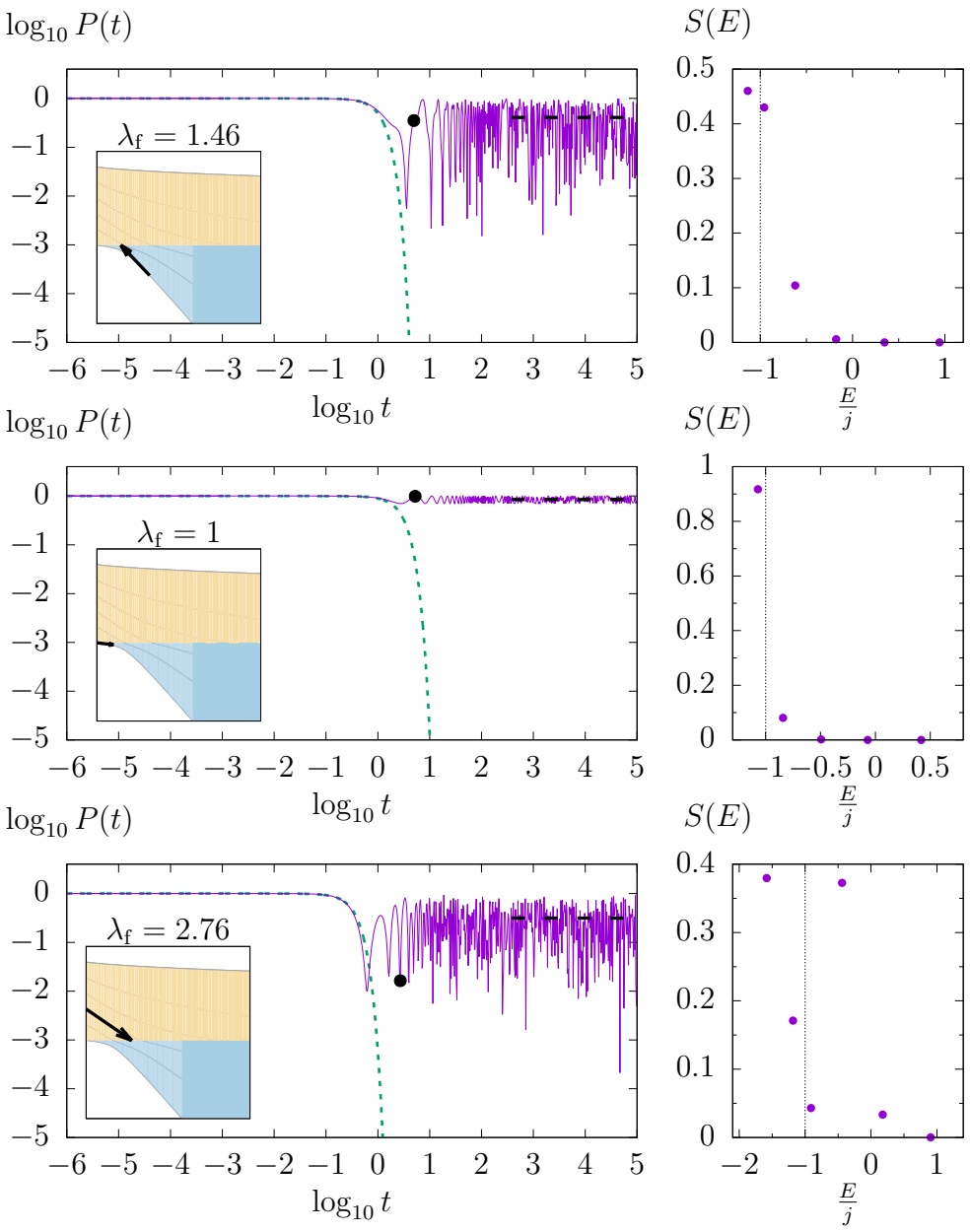

Figure B.14: Different quench protocols ending on the ESQPT borderline ($j = 5$)

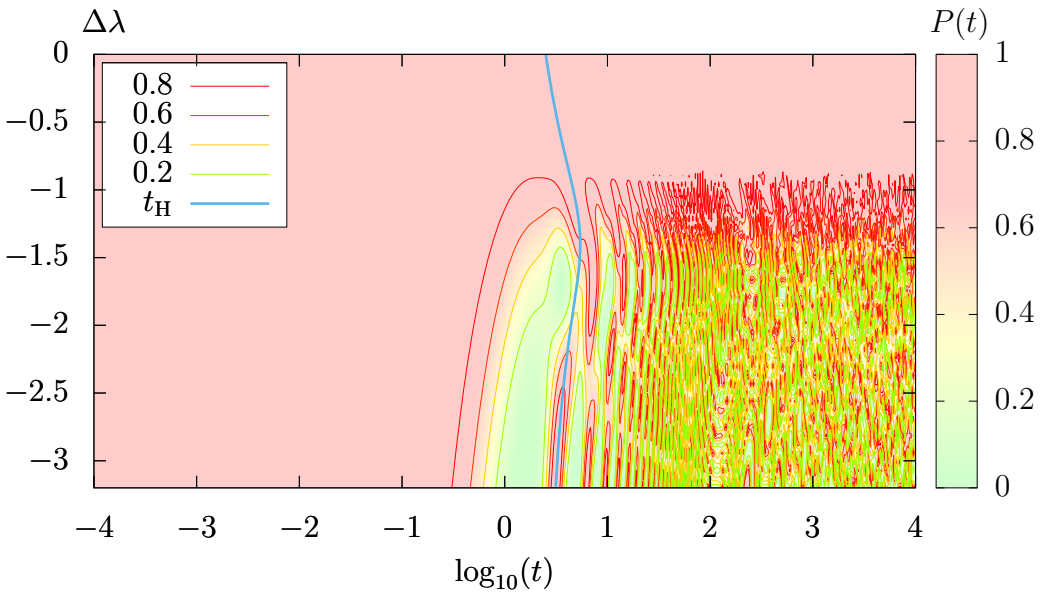

Figure B.15: Survival probability for ground-state BQPs starting from $\lambda_\mathrm{i} = 3.2$ as a function of the quench length $\Delta\lambda$ and time t ($j = 5$).

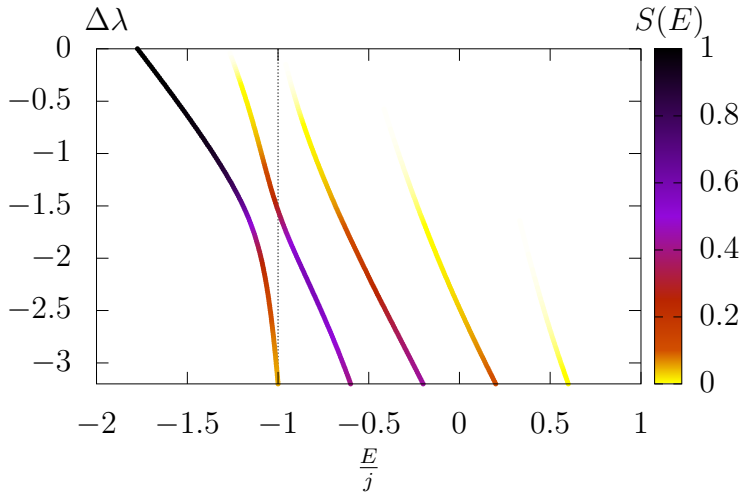

Figure B.16: Strength function for ground-state BQPs starting from $\lambda_\mathrm{i} = 3.2$ as a function of the quench length $\Delta\lambda$ and time t ($j = 5$).

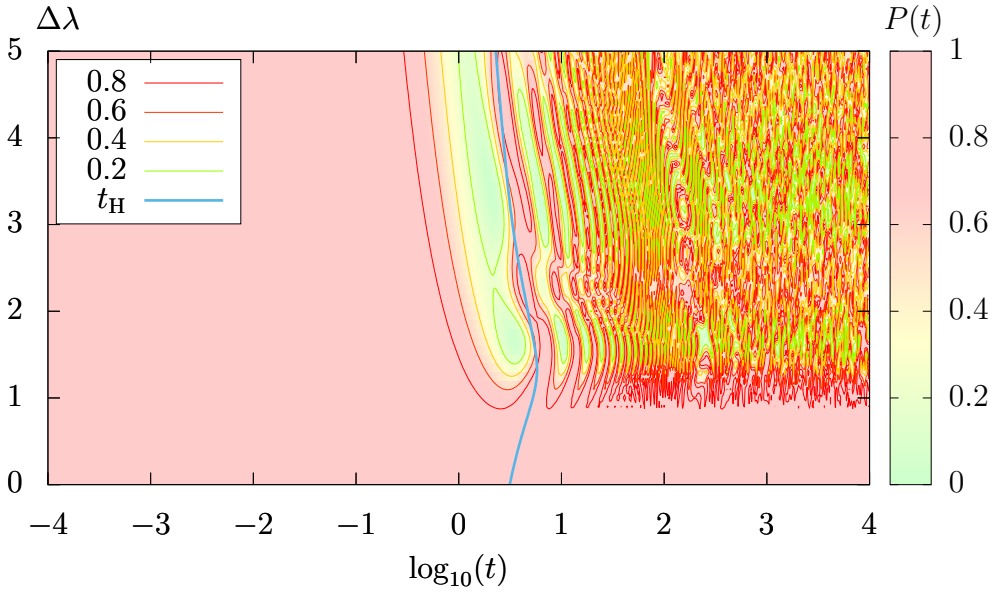

Figure B.17: Survival probability for FQPs from the ground state at $\lambda_{\mathrm{i}} = 0$ as a function of the quench length $\Delta\lambda$ and time t ($j = 5$).

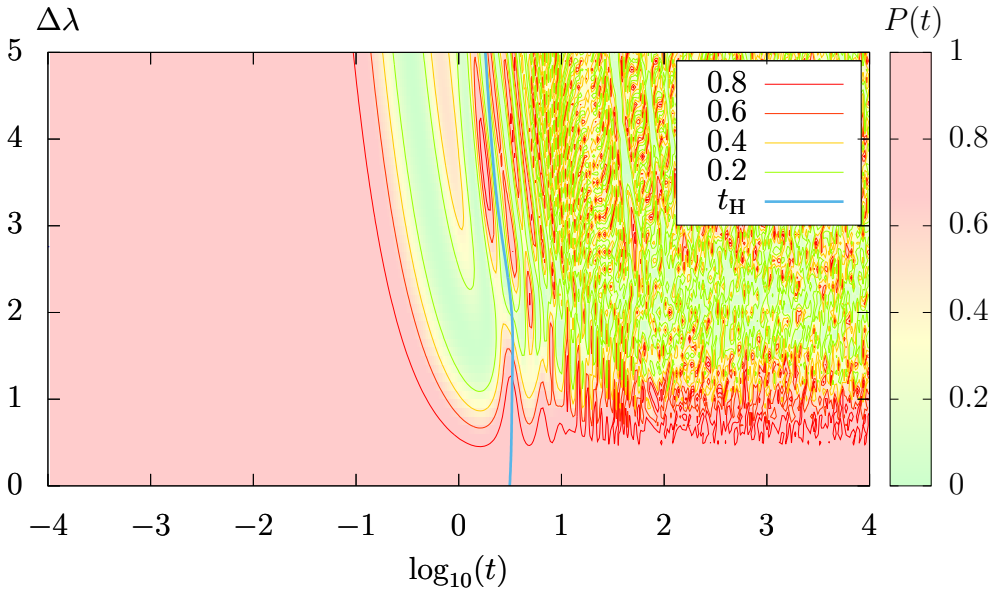

Figure B.18: Survival probability for FQPs from the middle-energy state of $\lambda_{\mathrm{i}} = 0$ as a function of the quench length $\Delta\lambda$ and time t ($j = 5$).

Bibliography

[1] P. Cejnar, P. Stránský and M. Kloc, *Physica Scripta* **90**, 114015 (2015).

[2] P. Stránský and P. Cejnar, *Physics Letters A* **380**, 2637 (2016).

[3] P. Cejnar and P. Stránský, *Physica Scripta* **91**, 083006 (2016).

[4] L. D. Carr, editor: *Understanding Quantum Phase Transitions*. Taylor & Francis, 2010.

[5] I. M. Georgescu, S. Ashhab and F. Nori, *Reviews of Modern Physics* **86**, 153 (2014).

[6] M. Kloc, P. Stránský and P. Cejnar: *Quantum quench dynamics in Dicke superradiance models* (to be published).

[7] L. F. Santos and F. Pérez-Bernal, *Physical Review A* **92**, 050101(R) (2015).

[8] H. J. Lipkin, N. Meshkov and A. J. Glick, *Nuclear Physics* **62**, 188 (1965); N. Meshkov, A. J. Glick and H. J. Lipkin, *Nuclear Physics* **62**, 199 (1965); A. J. Glick, H. J. Lipkin and N. Meshkov, *Nuclear Physics* **62**, 211 (1965).

[9] P. Stránský, M. Dvořák and P. Cejnar, *Physical Review E* **97**, 012112 (2018).

[10] M. Kloc, Master's thesis. Charles University, Faculty of Mathematics and Physics, Institute of Particle and Nuclear Physics. 2013.